1-1-2011

Acute Synaptic Activity Causes Differential miRNA Expression in the Drosophila melanogaster Larval Central Nervous System

Robert Ian Sand
University of Denver

Acute Synaptic Activity Causes Differential miRNA Expression in The *Drosophila melanogaster* Larval Central Nervous System

_____

A Thesis

Presented to

the Faculty of Natural Sciences and Mathematics

University of Denver

_____

In Partial Fulfillment

of the Requirements for the Degree

Master of Science

_____

by

Robert I. Sand

June 2011

Advisor: Dr. Scott A. Barbee

Author: Robert I. Sand
Title: Acute Synaptic Activity Causes Differential miRNA Expression in The *Drosophila melanogaster* Larval Central Nervous System
Advisor: Dr. Scott A. Barbee
Degree Date: June 2011

Abstract

The primary goal of this thesis was to determine if spaced synaptic stimulation induced the differential expression of microRNAs (miRNAs) in the *Drosophila melanogaster* central nervous system (CNS). Prior to attaining this goal, we needed to identify and validate a spaced stimulation paradigm that could induce the formation of new synaptic growth at a model synapse, the larval neuromuscular junction (NMJ). Both Channelrhodopsin- and high potassium-based stimulation paradigms adapted from (Ataman, et al. 2008) were tested. Once validation of these paradigms was complete, we sought to characterize the miRNA expression profile of the larval CNS by miRNA array. Following attainment of these data, we used quantitative real-time PCR (RT-qPCR) to determine if acute synaptic stimulation caused the differential expression of neuronal miRNAs. We found that upon high potassium spaced training in a wild type (Canton S) genotype, 5 miRNAs showed significant differential expression when normalized to a validated reference gene, the U1 snRNA. Moreover, absolute quantification of our RT-qPCR study implicated one miRNA: miR-958 as being significantly regulated by activity. Investigation into potential targets for miR-958 revealed it to be a potential regular of Dlar, a protein tyrosine phosphatase implicated in synapse development. This investigation provides the foundation to directly test our underlying hypothesis that, following spaced training, differential expression of miRNAs alters the translation of proteins required to induce and maintain these structural changes at the synapse.

Acknowledgments

Funding for this research was provided from a grant from NIH/NIDA**.** I would like to thank Dr. Scott Barbee for all of his support, direction and mentoring that contributed to this project. I would also like to Dr. Joseph Angleson and Dr. Robert Dores for their generous guidance and insight while serving on my thesis committee. For help with apparatus construction, electrical troubleshooting and mentoring, I would like to thank Dr. Nancy Lorenzon. For imaging troubleshooting and input regarding several aspects during the development of my project, I would like to thank Dr. J.T. Blankenship. For help with microdissection, RNA isolation and overall support, I would like to thank Leslie Rozeboom. For help with microdissection, image scrambling and guidance, I would like to thank Sarala Pradhan. Finally, for assistance in image scrambling and serving as kind helpers for various aspects pertaining to this project, I would like to thank Katherine Nesler and Breanna Symmes.

Table of Contents

CHAPTER ONE: BACKGROUND AND SIGNIFICANCE

1.1 Memory

The cognitive process of memory can be understood as retention, consolidation and recall of a particular input. This input can essentially be any event, observation or environmental stimuli that the organism can perceive. The interpretation of these inputs for later recall inherently divides them into to one of two major forms of memory called explicit memory. Explicit memory involves the conscious recollection of events and is a mechanism we use every day (Tulving, 2002). An example of this is the conscious retrieval of information from a lecture for use on a test. This differs from implicit memory where the retention and recall of an input is unknowingly performed. Consolidation and usage of this type of memory is based on repeated instances of the stimuli, and the ability to perform in a more in a consistent nature in response to this repetition in an unconscious fashion (Schacter, 1987). One real-life example of implicit memory is driving to work along the same route many times. Before long, you literally don't consciously debate over the path taken; it is implicitly recalled and executed. Together, these make up the foundational basis of how different memories are organized and recalled.

However, these processes do not explain how the initial stimuli are converted to a traceable memory. In terms of initial absorbance and later consolidation of the input, two more processes must be explained: short-term (STM) and long-term (LTM) memory.

Initial treatment of a stimulus first “passes through” the realm of short-term memory formation, and its candidacy for further consolidation is based upon relevance and impact. For example, listening to an entire lecture on proper noun usage, which is of no interest to the student, will still be able to be initially recalled. However, in a short amount of time the lesson will be forgotten, simply because it had no lasting impact to the student. This can also occur if several non-impacting stimuli are received, such as a lesson on every grammatical rule in the English language. Only most can be initially recalled but an ability to recall specifics will rapidly degrade over time. This is because short-term memory is inherently finite in capacity and retention time is inversely related to the amount of input received (Baddeley, et al. 1975). Research relating to this transient mechanism of short term memory has revealed that this process is indeed time-dependent and can truly be labeled as a temporary change. However, these temporary memories can be conserved via consolidation of stimuli in to a long-lasting form, known as long-term memory. One way information is intially learned is by repetition. In this implicit-like fashion, repeated exposure can commision the thought to the realm of long-term. This can be seen when studying how to spell and pronounce words. The more the child repeats and uses the word, the easier it is to recall in a subsequent spelling test (Baddeley, 1966). This model of repetative learning has also been experimentally repicated, promoting further work into LTM formation. Research to further understand these processes will shed light on the basic mechanisms underlying memory disorders such as dementia and age-related memory loss. Studies into how these two portions of memory formation occur at the cellular level have promped the advent of artifical induction of processes that resemble these classical descriptions, which will be discussed next.

1.2 Cellular mechanisms associated with memory

Experimental examination in to the process of STM formation has provided limited information in regards to the cellular process that occur. Pherhaps one of the best explanations for STM-genesis is with regards to neurotransmitter (NT) release and occupation into the synaptic cleft. Following initial stimulation in neurons, depolarization causes presynaptic exocytosis of neurotransmitters from the readily releasable pool (RRP). Levels of NT in the synaptic cleft and RRP capacity decrease over time. In a recent publication (Tarnow, 2009) the time course of RRP depletion following single stimulation correlated to the retention time for recall of newly learned words in human behavioral studies. This result suggests that STM may be readily controlled by RRP levels following initial depolarization. These data rienforce the observation that STM is a temporary condition, that eventually degrades.

In contrast to STM studies, research pertaining to LTM formation has generated a much larger interest and many subsequent findings. In fact, it has been suggested that the two processes are mutually exclusive (Izquierdo, et al. 1999). This research has focussed largely around implicit types of LTM formation due to development of artificial spaced stimulation paradigms that replicate this type of repetitive learning as previously described, although exceptions concerning behavioral conditioning paradigms relating to the same spaced training has provided support for an explicit basis (Barco, et al. 2006). The basis of this research developed from initial implications made by Donald Hebb (Hebb, 1949) in which he described the postulate that repeated signaling between two neurons led to subsequent long-lasting functional changes between them to reinforce the same type of communication in the future. This initial thought led to the further study

into synaptic plasticity, a process by which a synapse can alter its signalling dynamics in response to stimulation. To test this hypothesis, an artificial method of inducing LTM-like events was developed in mice hippocampal neurons (Bliss, 1979). The spaced electrical stimulation of neurons led to the discovery of activity-dependent long-term potentiation (LTP), described as a sustained increase in synaptic transmission strength (Kandel, 2001), which was due to modifications in levels of presynaptic active zones, postsynaptic neurotransmitter receptors or both. These changes could be quantified utilizing electrophysiological techniques to derive current traces.

Further studies described LTP to be subdivided into two phases: early- and late-phase LTP (E-LTP, L-LTP). These were differentiated both due to their primary modes of altering the synapse and their temporal location. The E-LTP phase was governed by the requirement for new protein synthesis, or translation (Frey, et al. 1996). The later L-LTP phase, L-LTP, was shown to be dependent on both translation and new transcription (Frey, et al. 1988). The total process would be on the time-scale of hours. Although this artificial induction of LTM-like changes in LTP has been debated (Martin, et al. 2000), it is now considered to be an accurate model for LTM albiet in an artificial sense. In addition to mammalian systems, development of similar spaced training paradigms in model organisms including *Drosophila* (Yu, et al. 2006) and *Aplysia* (Mauelshagen, et al. 1998) show the induction of the same type of long-term synaptic changes. Furthermore, evidence has supported the notion that in addition to strength, alterations in synaptic structure have been implicated in these LTM-associated spaced trainings (Ataman, et al. 2008; Chklovskii, et al. 2004; Wu, et al. 2001). These observations have led to the

understanding that synaptic plasticity as a whole is not soley based changes in synaptic efficacy, but in fact also may involve changes in synapse structure.

1.3 Molecular mechanisms associated with LTM

Regulation of the cellular processes addressing LTM formation, leading to alterations in synapse strength and structure, have been shown to involve several molecular players (Martin, et al. 2000). A myriad of kinases, cytoskeletal components, receptors, transcription factors and other components all feed in to the activity-dependent changes associated with LTM. For instance, changes in synapse strength were observed due to LTP-induced increases in AMPA receptors in dendritic spines (Malinow, et al. 2002). In addition, LTP-associated structural changes in rat hippocampal dendrites were inhibited when an actin antagonist was applied (Knucker, et al. 2000). Adding to this, the LIM-containing protein kinase (LIMK), necessary for activation of actin-polymerization, was shown to be essential in activity-dependent spine morphogenesis and memory formation associated with LTP (Luo, 2002). Finally, it has been determined by several studies that elimination of the transcription factor CREB aboloshes activity-dependent LTP and LTM-associated changes (reviewed in Benito, et al. 2010). Taken together, these various molecular mechanism regulating LTM should only be considered as a fraction of all the regulators pertaining to the process. Since this is by nature an activity-dependent process, activity-induced regulators of these molecular processes must be considered. To this extent, a recent body of work (Kosik, 2006) has implicated microRNAs (miRNAs) as potential regulators of these downstream effectors of synaptic plasticity.

The molecular mechanisms associated with LTM have been shown to have regulatory input from miRNAs (Ashraf, et al. 2006; Berdnik, et al. 2008). Evidence has suggested that the RNA induced silencing complex (RISC)-mediated miRNA pathway is required for early phase LTM, by way of governing local protein synthesis at the synapse. Recently it was shown in (Ashraf, et al. 2006) that one of the more important regulators of synaptic plasticity, the calcium/calmoduln-dependent protein kinase II (CaMKII), was translationally regulated by a RISC-dependent event locally at synapses in *Drosophila*. Subsequent miRNA targeting predictions of the CaMKII 3'-UTR revealed possible binding sites for miR-280 and miR-289. While miRNA regulation in this early stage has relevance, the late-phase of LTM, which requires transcription is a more likely area to investigate for miRNA-mediated LTM. Recently, (Fiore, et al., 2009) demonstrated that an activity-dependent miRNA successfully regulated *pumilio* in rat cortical neurons, a protein responsible for aiding in long-lasting changes at synapses. This presents the ability of a miRNA to undergo activity-induced transcription which then would act to regulate mRNA transcripts associated with activity-dependent LTM associated changes.

1.4 Charactarization of miRNAs: Biogenesis and Translational Regulation

microRNAs are a class of small non-coding single stranded RNAs (ssRNA) that have been implicated in the process of translational regulation and mRNA degradation (Kosik, et al. 2005; Kosik, 2006). The biogenesis of a mature 20-22nt miRNA begins with transcription via RNA polymerase II (Lee, et al. 2004) of the much longer pri-miRNA sequence, whose structured hairpin facilitates the subsequent binding of the RNAseIII protein Drosha (Kim, et al. 2009). Drosha, in combination with the dsRNA binding protein Pasha, form the microprocessor complex (Denli, et al. 2004) which works

to cleave the hairpin structure, creating a double stranded pre-miRNA (Summarized in Appendix I, Supplemental Figure 7). Following cleavage, the transport protein, Exportin 5 shuttles the pre-miRNA out of the nucleus and in to the cytoplasm (Lund, et al. 2004). There, the RNAseIII enzyme Dicer then cleaves the pre-miRNA product into two separate strands, the normal and the star (*) strand. Although each has the capability of binding to completely separate mRNA targets by loading on to RISC, the star strand is usually degraded. Recent evidence suggests thermodynamic favorability of one strand over the over might be responsible for this selection (Khvorova, et al. 2003). Once this mature miRNA is formed, it must receive aid to perform its regulatory job (Kosik, 2006). The RISC is a collection of proteins, including Argonaut (Ago), which deliver the miRNA to its target mRNA. The process of miRNA mediated translational regulation can occur in one of two ways: repression or degradation. In the repression role, the mature miRNA binds to a small 7-8 nt site of perfect complementation on the 3'-UTR of its target mRNA. This region binds to the conserved "seed region" of the miRNA. This binding holds the miRNA-RISC complex to mRNA transcript. (Wahid, et al. 2010) presents 4 general methods by which this repression may occur. First, the associated complex may sequester the 5' cap of the mRNA, not allowing association with the eIF-associated translational machinery. The second method may be the miRNA-RISC complex sequestering the eIF6 complex, thereby preventing full association of eIF complex required for translation. The third method suggests that the bound miRNA-RISC does not allow for mRNA circularization, a requirement for translational activiation. Finally, in a post-initiation phase, the miRNA-RISC association with the mRNA may cause "pre-mature ribosomal dropoff." In all of these proposed methods of repression,

these in turn would silence the mRNA translation. miRNAs have recently been shown to act in conserved mRNA degradation pathways (Fabian, 2010). In the same manner of recruitment and binding as in the repression pathway, complementation of binding along the 3'-UTR of the target mRNA can lead to deadenlyation, decapping, and 5'-to-3' exonucleolytic degradation. Through either of these mechanisms, we predict that activity-regulated miRNAs may bind to and control expression of target mRNAs whose protein products are involved in LTM-associated synaptic alterations.

1.5 Summary

In this thesis we attempt to identify novel regulatory mechanisms that may be involved in the formation of immediate and lasting synaptic alterations associated with LTM. Our hypothesis is that, following activity stimulation, differential expression of a subset of neuronally specific miRNAs will lead to the translational regulation of proteins important to the process of LTM. First, we provide experimental evidence of a validated stimulation paradigm previously shown to induce rapid, activity-induced structural changes at a model glutamatergic synapse in *Drosophila melanogaster* (Ataman, et al. 2008). Then, we characterize the miRNA expression profile in the larval CNS. Finally, we show upon acute spaced stimulation, statistically significant down-regulation of 5 neuronal miRNA occurs in the larval CNS, all of which are predicted to regulate developmental synapse-related proteins. One protein in particular, Dlar, is predicted to be controlled by 3 activity-dependent miRNA including the strongest induced miR-958.

CHAPTER TWO: LIGHT-INDUCED SPACED TRAINING PARADIGM AND MIRNA PROFILING BY MIRNA ARRAY

2.1 Introduction

Investigation surrounding the molecular mechanisms regulating long-lasting structural changes at the synapse has prompted the increased usage of *Drosophila* as a powerful model system. The use of the larval neuromuscular junction (NMJ) has emerged due to its size, accessibility, ease of genetic manipulation, and its inherent ability of being a highly plastic synapse (Schuster, 2006). Recently, (Ataman, et al. 2008) demonstrated that it is possible to induce rapid activity-dependent changes at the NMJ utilizing a light-based spaced training paradigm in intact, living *Drosophila* larvae by taking advantage of the selective light-gated cation channel, Channelrhodopsin-2 (ChR2). ChR2 was originally discovered in the green alga *Chlamydomonas reinhardtii* (Nagel, et al. 2002; Nagel, et al. 2003) and has been speculated to be involved in the process of phototaxis, similar to other reported channelrhodopsins (Schmies, et al. 2001). Transgenic expression in *Xenopus* oocytes showed that in the presence of the light isomerized chromatophore all-trans-retinal, necessary for proper channel assembly; light activation (~470 nm, blue) caused large cation currents (Nagel, et al. 2003). Expression of ChR2 in tissues of other model systems has shown this channel to be effective in both mammals (Nagel, et al. 2003) and flies (Schroll, et al. 2006).

ChR2 can be expressed in *Drosophila* neurons using a neuron-specific GAL4 driver in combination with the UAS/GAL4 expression system (Brand, et al. 1993). Using this approach, it has been demonstrated that transgenic ChR2 can selectively activate subpopulations of neurons (Schroll, et al. 2006). (Ataman, et al. 2008) found that light-induced spaced training of intact transgenic larvae expressing the ChR2 in motor neurons caused synapse depolarization and long-lasting changes in synapse structure. This paper revealed that approximately 1 hour following spaced training, the development of immature synaptic boutons, termed "ghost boutons" was observed at the larval NMJ (Ataman, et al. 2006). These structures positively reacted to the presynaptic marker horseradish peroxidase (HRP), but were devoid of postsynaptic structures, marked by proteins such as the *Drosophila* PSD-95 homologue Discs Large (DLG). These ghost boutons were shown later to develop into mature synaptic boutons. Of particular interest to the work presented in this thesis, this paper demonstrated that formation of ghost boutons at the NMJ is dependent on both transcription and translation.

Activity-dependent control of new gene transcription and mRNA translation is required for consolidating and maintaining long-lasting changes at the synapse associated with LTM. miRNAs have been shown to be regulators of translation and are thought to be key players in synaptic plasticity (Ceman, et al. 2011; Vo, et al. 2010). Moreover, the ability of miRNAs to regulate activity-dependent dendritic plasticity in both *Drosophila* and mammals has been well established (Berdnik, et al. 2008; Schratt, et al. 2006; Wayman, et al. 2008; Fiore, et al. 2009). Based on these data, we predicted that the transcription of specific miRNAs involved in the control of synaptic plasticity might be

differentially expressed in response to acute synaptic activity. In turn, these miRNAs may serve as regulatory mechanisms to control the expression of proteins involved in the process of LTM-associated structural plasticity.

The objective of the experiments presented in Chapter 2 was to identify activity-regulated miRNAs following light-activated stimulation via ChR2. In our hands, we found that while ChR2 stimulation increased the number of ghost boutons at the larval NMJ, this increase was not statistically significant. Moreover, using this stimulation paradigm, we did not observe significant changes in miRNA expression profiles compared to un-stimulated controls using a miRNA microarray (Exiqon A/S). Despite these negative results, using this approach we were able to identify all miRNAs expressed in the larval CNS.

2.2 Results

2.2.1 Activity-dependent structural changes are not observed at the NMJ following light-induced synaptic stimulation.

To examine activity-dependent changes in synapse structure in *Drosophila*, we first constructed an apparatus capable of inducing light-activated muscle contractions in intact ChR2 transgenic larvae (Appendix I, Supplemental Figure 1; data not shown; (Schroll, et al. 2006; Ataman, et al. 2008). Published findings have shown a statistically significant ($p < 0.001$) 2.5-fold increase in the number of ghost boutons at the larval NMJ on muscles 6/7 (m6/7) in abdominal segment 3 (A3) following an acute spaced stimulation paradigm (Figure 1A; data not shown). In a misinterpretation of this

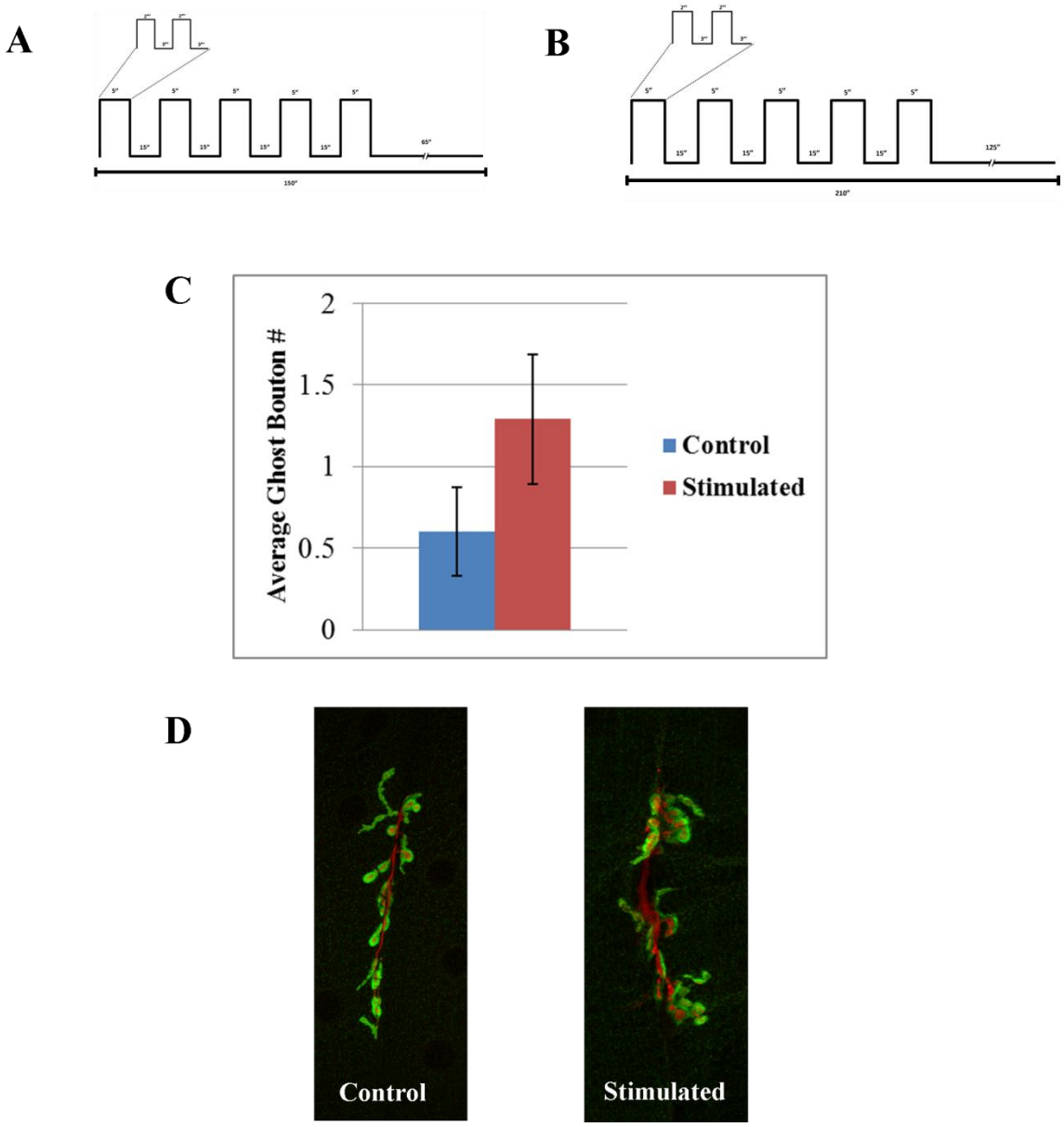

Figure 1- Light-induced spaced training of ChR2 transgenic larvae does not induce significant formation of ghost boutons. (A) The 2-hour original spaced stimulation paradigm utilized in (Ataman, et al. 2008). (B) The 3-hour misinterpreted stimulation paradigm used for our ChR2 based experiments. (C) Ghost bouton quantification following light-induced spaced training in transgenic C380-ChR2 larvae. Control (n=15), stimulated (n=14), p=0.17. Although a 2.14-fold change in ghost bouton formation appears, no significance is reported. Error bars are +/- SEM. (D) Representative images of A3 M6/7 for both treatments in light-induction study. Images collected using a 60x objective on a scanning confocal microscope.

paradigm, we used a modified approach that allotted an extra hour following the last stimulation (Figure 1B). Quantification of our larval NMJs (n=15) revealed a trend towards a > 2-fold increase ghost bouton number (Figure 1C). Although ghost boutons were observed, there was no significant difference relative to control ($p = 0.17$; Figure 1D). We repeated this experiment two times and found results consistent with the initial experiment (data not shown). Together, these data imply that ghost boutons appear to form in response to acute light-induced synaptic stimulation. However, our results are not statistically significant. Perhaps this was because our stimulation paradigm differed from the published paradigm.

2.2.2 Activity-dependent changes in miRNA expression are not observed in the larval CNS following light-induced synaptic stimulation.

In a desire consistent with other published works (Park, et al. 2009; Wibrand, et al. 2010), we wished to identify, via microarray, potential miRNA that were regulated by spaced training in the *Drosophila* CNS. Total RNA of CNS tissues was isolated from w^{1118}, UAS-ChR2 (stimulated), and UAS-ChR2 (un-stimulated) non-wandering 3rd instar larvae and sent off for miRNA microarray analysis (Exiqon A/S). The *Drosophila melanogaster* miRNA array chip represented 62% coverage of known miRNAs in the current miRBase 17.0 registry (Griffiths-Jones 2004; Griffiths-Jones, et al. 2006; Griffiths-Jones, et al. 2008; Kozomara, et al. 2011). An arbitrary 2-fold cut-off in differential expression was set for biological relevance. The microarray revealed that between stimulated and control samples, no miRNA was found to be differentially expressed above our threshold. Since the same modified ChR2 stimulation paradigm was

used as in the ghost bouton study (Figure 1B), this may have explained the results obtained. Moreover, we have missed identifying some miRNAs because the available microarray chip covered 62% of the currently annotated miRNAs in the fly genome. Interestingly, we did observe a > 2-fold change of 6 miRNAs between the w^{1118} control and UAS-ChR2 control samples (Appendix II, Supplemental Table 1A). This is probably due to genotypic variation between w^{1118} and *UAS-ChR2*. We reset our cut-off to be > 1.1-fold change and found 20 miRNAs to meet these criteria (Appendix II, Supplemental Table 1B) with miR-314 having the greatest differential expression of -1.44-fold.

Due to the notorious variability of microarray data, validation of these results must be performed using the more sensitive reverse-transcription quantitative real time PCR (herein referred to as RT-qPCR). RT-qPCR validation of suspected microarray identified activity-dependent miRNAs revealed inconsistent results. Utilizing the same UAS-ChR2 genotype and light induced paradigm (Figure 1B), 3rd instar larvae underwent either 5x spaced training or 0x (control). 2 reference genes for data normalization, U12 snRNA and U76 snRNA, were then tested in both samples in triplicate utilizing RT-qPCR. Data were normalized using $\Delta\Delta C_t$ relative quantification. These resultant data (Figure 2A) indicated a very different expression profile compared to the original microarray data. These data revealed that 9 of the tested miRNA exhibited induction in the opposite direction. Even though some miRNA underwent differential expression following spaced training greater than 2-fold, these results were cautiously considered. First, regression analysis between the miRNA array and RT-qPCR experiments (Figure 2B) showed very poor correlation between results and was not significant

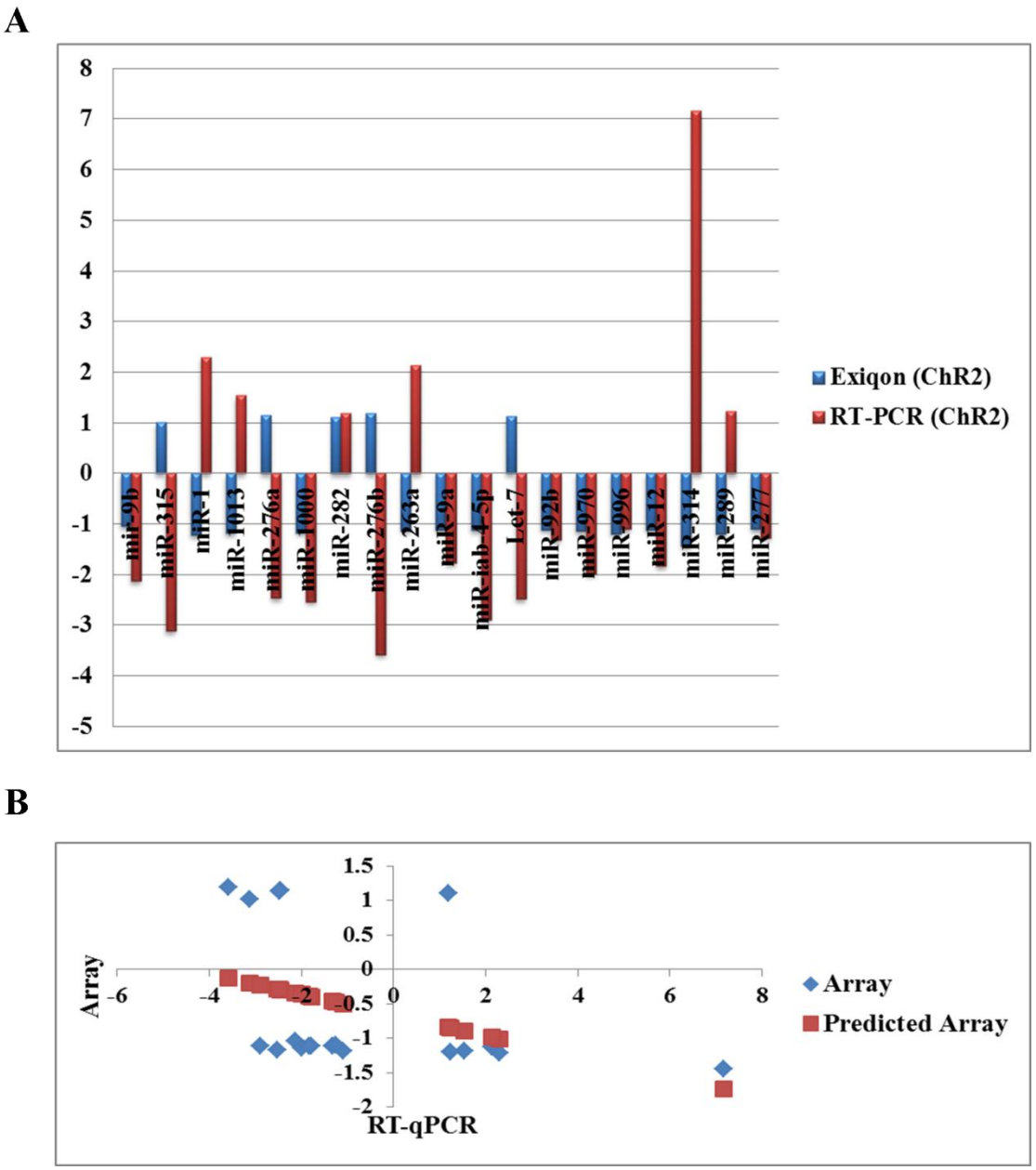

Figure 2-RT-qPCR validation of the ChR2 based microarray experiment reveals conflicting results. (A) RT-qPCR fold change summary shows a result conflicting with the majority of the initial findings. Data was normalized to U12 snRNA and u76 snRNA and relatively quantified using the $\Delta\Delta C_t$ method. (B) Regression analysis plot revealed an insignificant (p=.10)(R=0.38) correlation between microarray data and subsequent RT-qPCR validation. Regression analysis was performed using the Excel Analysis Toolpak.

(R=0.38, p=0.10). Second, a statistically significant increase in ghost bouton formation was not observed following ChR2 stimulation (Figure 1C-D). Based on these two observations, no definitive conclusion could be drawn. However, the miRNA microarray data did reveal that 79 miRNA were expressed in the larval CNS (Figure 3). Thus, we did successfully identify the miRNA expression profile of the larval CNS. The full list can be found in Appendix III.

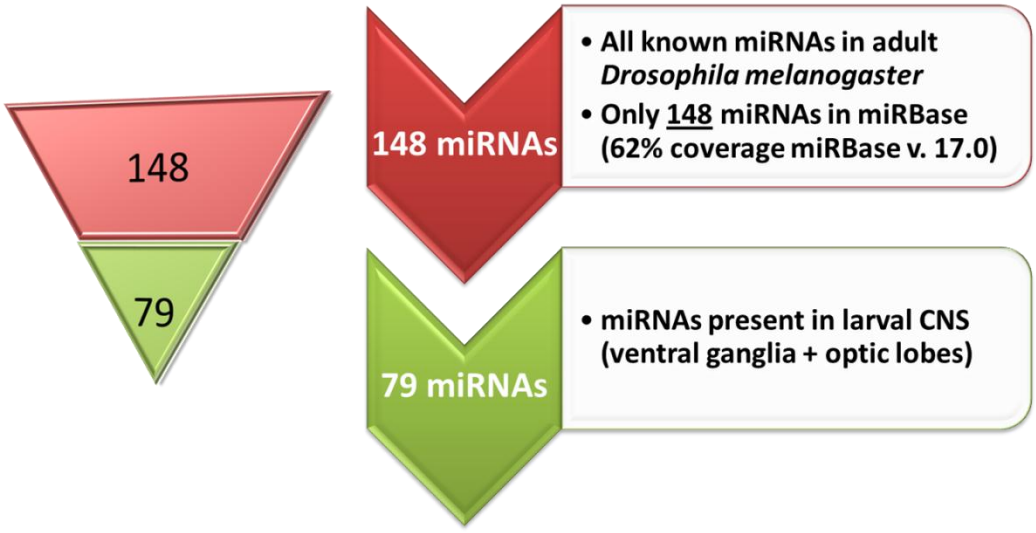

Figure 3- Determination of *Drosophila* 3rd instar larval CNS miRNA expression profile. This flow diagram depicts the microarray screen that was performed to determine CNS-specific miRNAs. The total miRNAs available for testing represents 84% of the overall coverage of miRNAs known in *Drosophila* since the release of miRBase 17.0.

CHAPTER THREE: HIGH POTASSIUM SPACED TRAINING PARADIGM AND MIRNA PROFILING BY RT-QPCR

3.1 Introduction

In the wake of the miRNA expression studies utilizing ChR2 light-based spaced training, three major caveats developed. First, as mentioned in the miRNA microarray results, significant differences between un-stimulated UAS-ChR2 and w^{1118} control samples were observed. This indicated that genotypic effects might be leading to altered miRNA expression profile. Second, the ChR2 stimulation paradigm previously found to significantly induce the desired LTM-associated long-lasting changes in synapse structure (Ataman, et al. 2008) was different from the one that we used (Figures 1A-B). This was indicated by our experiments where this modified paradigm did not significantly induce rapid and long-lasting structural changes at the NMJ (Figure 1C). Finally, the ChR2 light induced paradigm has been shown to produce significantly weaker phenotypes than other stimulation paradigms (Ataman, et al. 2008). For these reasons the light-based stimulation paradigm and indeed use of the UAS-ChR2 genotype was abandoned.

One of the more traditional methods of spaced training, particularly in eliciting cellular and molecular effects associated with LTM, has been through the application of hyperkalemic buffers (Wu, et al. 2001). This potassium (K^+)-dependent stimulation causes non-specific neuronal depolarization, and when applied in specific intervals, this

spaced depolarization can cause long-lasting synaptic changes. This method of induction was previously utilized by (Ataman, et al. 2008) in experiments where spaced training led to an increase in the number of ghost boutons in dissected *Drosophila* larval preparations. Their results revealed a near 6-fold increase in the number of ghost boutons present at the same larval NMJ at segment A3 m6/7. These highly significant results ($p < 0.0001$) indicated that this type of stimulation is not only capable of inducing long-lasting structural changes at the synapse, but that it does so in a more robust fashion than the ChR2-based stimulation paradigm. Therefore, our new approach was to utilize the K^+-dependent stimulation paradigm.

In Chapter 3, we investigated the validity of the high potassium stimulation paradigm to induce ghost bouton formation in two genotypes: w^{1118} and "wild-type" Canton S. We found that successful induction did occur in both genotypes, validating the stimulation paradigm. In addition, we investigated, in both genotypes, the potential for the transcriptional up- or down-regulation of activity-dependent miRNA expression. We report first that, in an un-optimized experiment, the w^{1118} genotype elicited 8 miRNAs to induce >2-fold differential expression following stimulation. Then, following several optimization steps, we confirm differential expression following LTM-associated spaced training leads to statistically significant differential expression in the Canton S genotype of a subset of these CNS-specific miRNAs.

3.2 Results

3.2.1 High potassium spaced training causes rapid structural changes at the w^{1118} NMJ

With the decision to switch to the high potassium-based spaced training we wished to determine if this stimulation using a common lab control line, w^{1118}, could elicit these activity-dependent structural changes at the NMJ previously reported in (Ataman, et al. 2008). This line is often used in the lab as a control because most transgenic lines are constructed in this genetic background. Consequently, another stimulation apparatus had to be constructed, a perfusion-based buffer delivery system (Appendix I, Supplemental Figure 2). Using the published stimulation paradigm (Figure 4A), non-wandering, unstretched, semi-intact w^{1118} 3rd instar larvae underwent this high K^+ spaced training and were then subsequently fixed and imaged. Our results indicated that following high potassium spaced training, a 5.5-fold increase in ghost bouton number occurred at the larval segment A3 m6/7 NMJ although the actual numbers in controls vs. stimulated were lower (Figure 4B). Statistical analysis of the dataset (n=16) proved it to be significant ($p < 0.05$). Representative images of both stimulated and control NMJs exhibited ghost bouton formation (HRP^+ and DLG^-) (Appendix I, Supplemental Figure 3). These results provided the anticipated validation that rapid structural synaptic change can occur at the larval NMJ in the w^{1118} genotype following high potassium spaced stimulation.

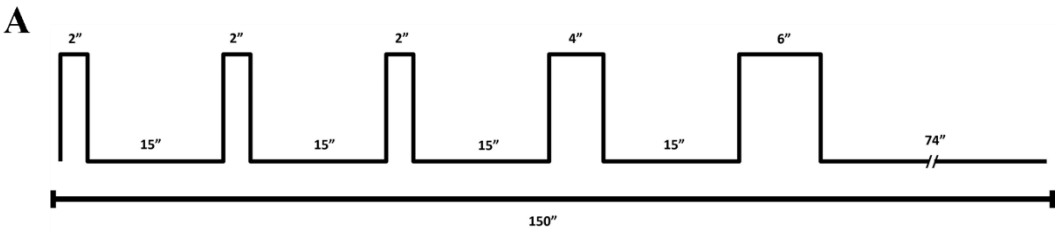

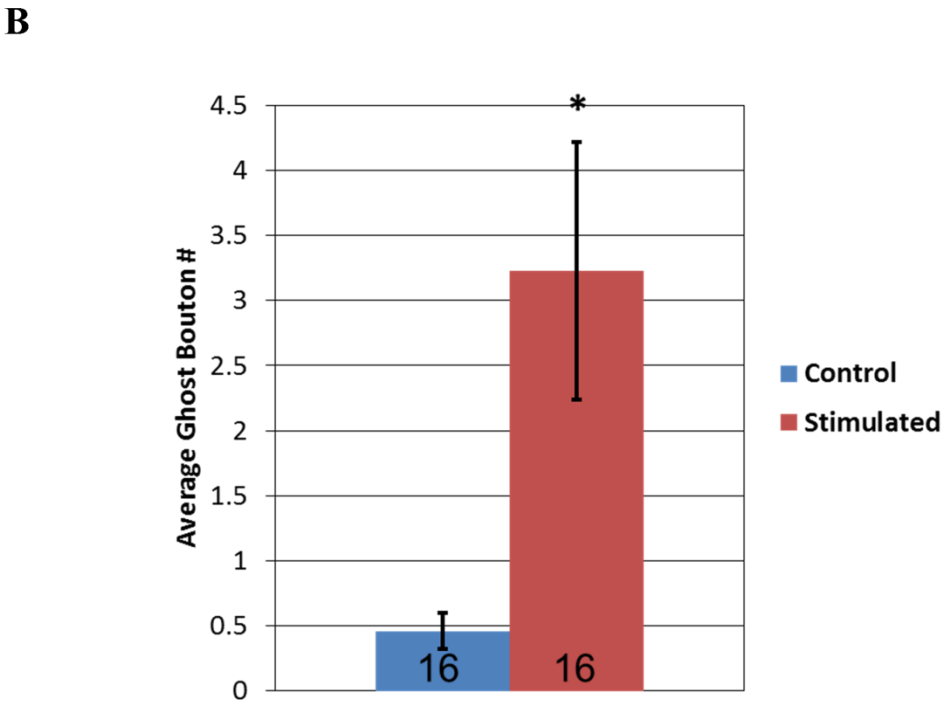

Figure 4- High potassium based spaced training leads to significant induction of ghost bouton formation in w^{1118} larvae. (A) Potassium based stimulation paradigm previously used in (Ataman, et al. 2008). This same paradigm was used in all high potassium based stimulation experiments. (B) Graph representing average ghost bouton formation following 5x spaced training. n=16 and ghost boutons were quantified from A3 M6/7. Student t-test found significance (*$p<0.05$). Error bars represent +/- SEM.

3.2.2 Activity-dependent changes in miRNA expression are observed in the w^{1118} larval CNS following high potassium-induced synaptic stimulation.

The initial RT-qPCR study that investigated activity-dependent changes in miRNA expression in the ChR2 larval CNS provided inconclusive evidence. First, the protocol used for ChR2 spaced training was inconsistent from previously validated paradigms (Ataman, et al. 2008), which may have led to a temporal bias in miRNA expression (Figure 1B). Second, the microarray revealed the highest miRNA expression differences to be between UAS-ChR2 control and the lab control line w^{1118} (Appendix II, Supplemental Table 1A). These results may indicate a possible genotypic variation relating to miRNA expression that could have caused skewed results. These findings prompted us to make two major changes to the experiment. First, we altered the stimulation paradigm and genotype, high potassium stimulated w^{1118}, whose combination was validated above (Figure 4B). Second, with the miRNA associated genotypic interactions between UAS-ChR2 and w^{1118}, we decided to abandon the focused list of miRNAs determined by the ChR2-based studies and retest all CNS-specific miRNAs for activity-dependent differential expression.

In order to facilitate this approach, a primer plate was obtained containing primer probes for all 79 miRNAs present in the larval CNS. In addition, 5 putative normalization controls: U1 snRNA, U5 snRNA, U12 snRNA, U76 snRNA and 185 snoRNA primer sets were also obtained. RNA from CNS tissues explanted from 3rd instar w^{1118} larvae was isolated. This isolation constituted a single biological replicate (n=1). Following reaction setup, the samples underwent RT-qPCR in technical triplicate. Data was normalized

using the standard $\Delta\Delta C_t$ relative quantification method. The results (Figure 5) indicated that 4 miRNAs: miR-282, miR-314, miR-12 and miR-304 underwent > 2-fold decrease in expression approximately 1 hour after spaced training. Again, this 1-hour timeframe is different than our previous ChR2 studies, which allowed 2 hours from the final stimulation. In addition, 4 miRNAs: miR-79, miR-8, miR-279 and miR-iab-4-5p showed > 2-fold increase in expression. It was discovered that U12 snRNA and U76 snRNA where normalized to the other controls exhibited apparent activity-dependent differential expression. Therefore, U12 and U76 were eliminated as controls in all subsequent experiments.

3.2.3 Activity-dependent structural changes are observed at the Canton S NMJ following high potassium spaced synaptic stimulation.

Following the promising results obtained from the w^{1118} RT-qPCR study, we decided to shift to the more wild-type genotype, Canton S. This decision was made based on NMJ morphology results from our lab which indicated that the w^{1118} NMJ exhibited an increased number of synaptic boutons and overall synapse size relative to many other genotypes (data not shown). This may be due to the accumulation of genetic modifiers picked up over the lifetime of the w^{1118} laboratory strain. These modifiers may cause skewed results when examining mechanisms that effect synaptic morphology, such as miRNAs. Since our aim is establish unbiased findings in activity-dependent miRNA-mediated synaptic development, we decided to pursue the Canton S genotype with which to conduct further studies.

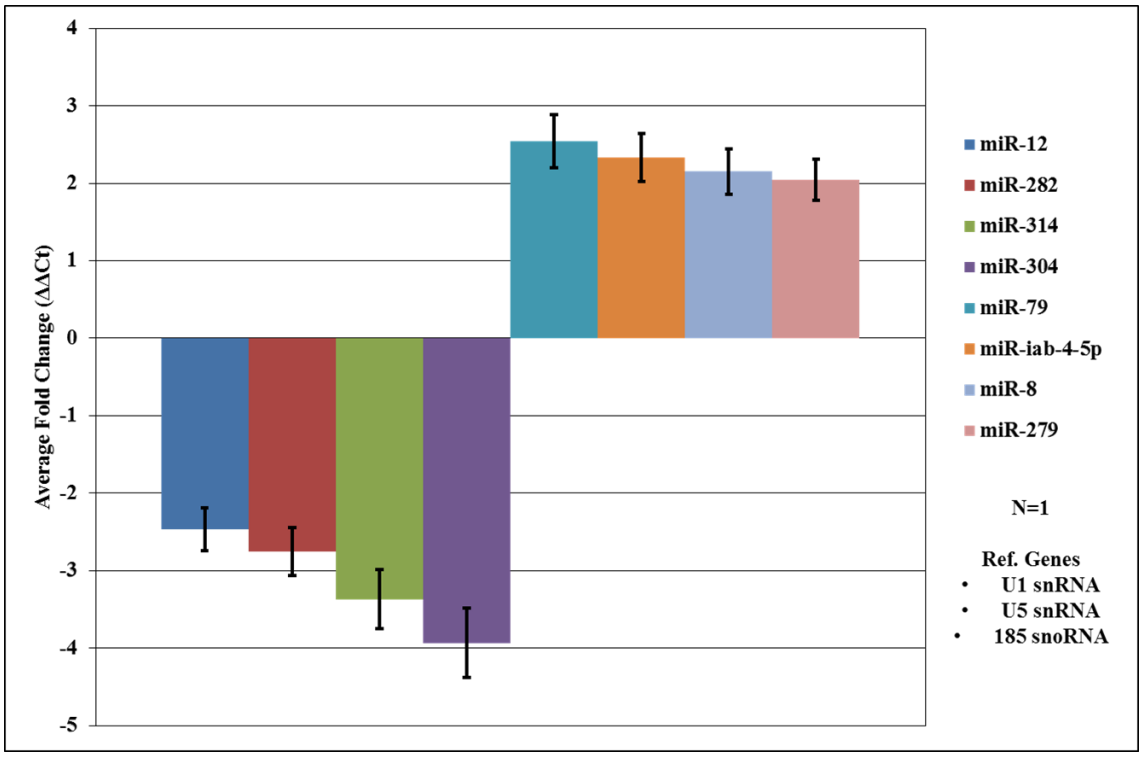

Figure 5- High potassium spaced training in w^{1118} larval CNS induces differential expression of 8 miRNAs. This resultant graph of a RT-qPCR study reveals differential expression of 8 CNS specific miRNAs, 4 positively regulated and 4 negatively regulated. Data was normalized to a pooled value of U1 snRNA, U5 snRNA and 185 snoRNA, and quantification was performed using the $\Delta\Delta C_t$ method. Error bars are +/- SEM.

Again, in our initial experiments, we attempted to replicate a published spaced training stimulation protocol using high potassium (Ataman, et al. 2008). Moreover, this experiment proved to be a better validation for the results reported in (Ataman, et al. 2008) since this was the actually the genotype used in their high potassium spaced training studies (not w^{1118}). Using non-wandering, unstretched, semi-intact Canton S 3rd instar larvae, high potassium spaced training (Figure 4A) was performed followed by fixation, immunostaining, and imaging. Our results indicated a 6-fold increase in ghost bouton number relative to un-stimulated controls occurred at the larval segment A3 m6/7 NMJ (Figure 6A). Statistical analysis of these resultant data (n=20) indicated that this was a highly significant result ($p < 0.0001$). These results were essentially identical to those previously reported by (Ataman, et al. 2008). Larval NMJs shown in Figure 6 were selected to demonstrate, with high clarity, the ability of this stimulation paradigm to strongly induce ghost bouton formation (Figure 6B). These images in particular did not represent the average findings of both control and 5x stimulated groups but, in the case of the latter, show the more robust-end of the total samples. The justification for this was that these two images showed very well defined ghost boutons with the majority having clear circumferential edges. These NMJs in particular demonstrate accurate ghost bouton size due to image clarity. Based on these scaled images alone, we observed these structures as having diameters with a range of 2-3μm (data not shown). Taken together, these results indicated that spaced training using high potassium dissection buffers caused significant formation of rapid structural changes at the larval NMJ in the Canton S genotype. With the validation of the Canton S genotype, subsequent RT-qPCR studies

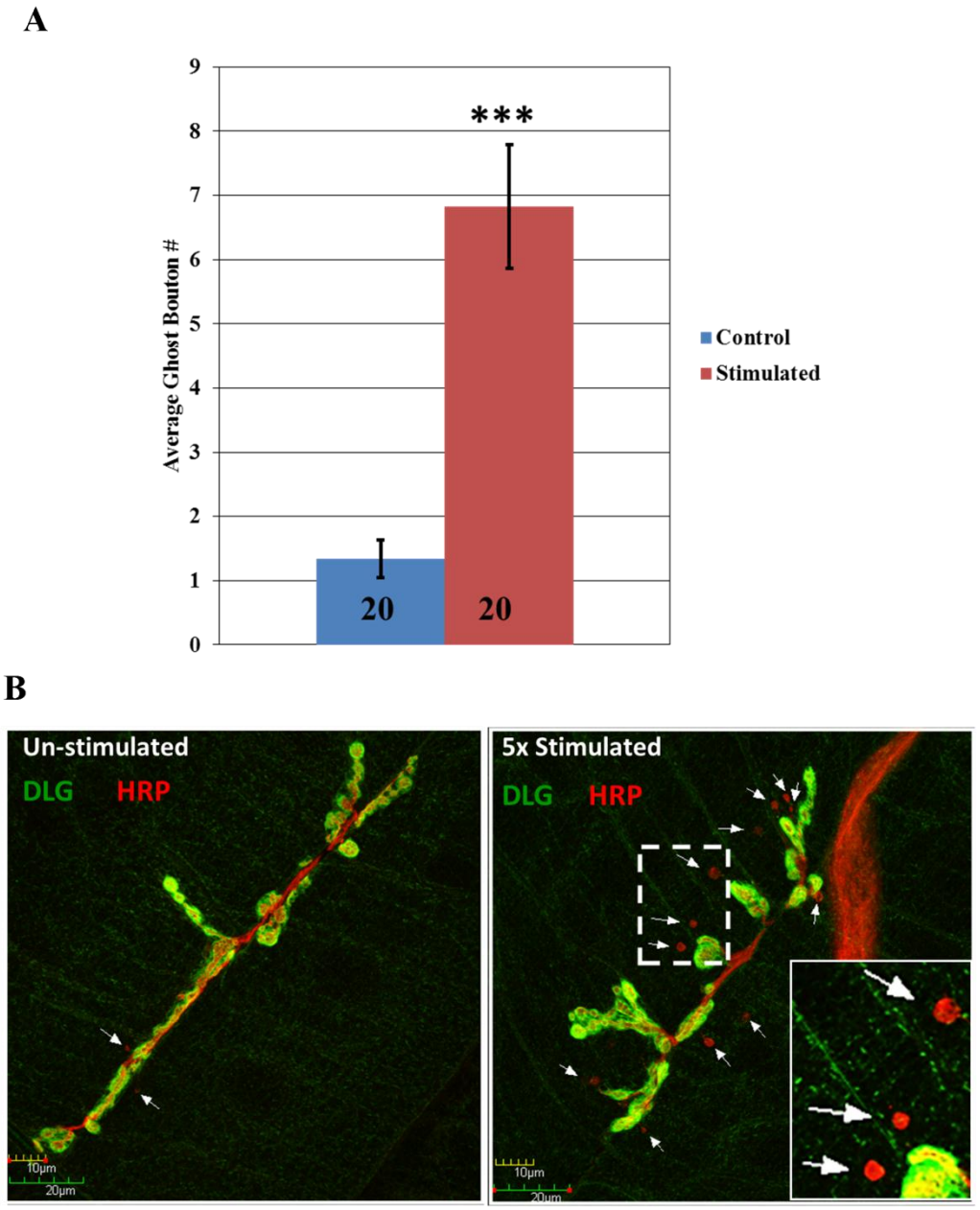

Figure 6- High potassium spaced training leads to significant ghost bouton formation at the larval NMJ in Canton S. (A) Resultant graph showing a 6 fold increase in ghost bouton formation following stimulation. Student t-test of the dataset revealed that the induction was highly significant (***$p<0.0001$). Error bars are +/- SEM. (B) Scaled images depicting robust induction in stimulated samples and control samples. Ghost boutons are labeled with arrows. Green= postsynaptic DLG, Red= presynaptic HRP. Scales are shown to judge ghost bouton diameters.

were performed in an effort to create a more accurate activity-dependent miRNA expression profile. Prior to such studies, however, a further effort to ensure unbiased results must be performed, specifically optimizing our miRNA RT-qPCR assay.

3.2.4 RT-qPCR Optimization

The power of RT-qPCR to detect and quantify minute sample amounts has prompted its increased use in genetic studies, especially in development. Results obtained from comparison of treatment conditions, such as our spaced stimulation studies, allowed determination of fold changes. An accurate and valid result generated from this system requires knowledge and optimization of specific parameters within the assay. Unfortunately, this practice is not common among researchers, which in turn can lead to ambiguous or inaccurate results that become detrimental to the scientific knowledgebase. Based on this, the establishment of a set of guidelines has occurred, which still unfortunately is still not widely practiced.

The recently published minimum information for quantitative real-time PCR experiments guidelines (MIQE) (Bustin, et al. 2009; Bustin 2010) has proposed standardization for RT-qPCR studies. These guidelines explicitly documented several publications that have provided data from non-validated RT-qPCR studies that have proven incorrect. As a result, methodologies such as RNA integrity analysis, primer efficiency analysis, and melt curve analysis have been labeled paramount for assuring validity of results. While some of these guidelines are potentially superfluous, these aforementioned requirements are in reality quite paramount for any RT-qPCR study. To

this extent we devised a set of experiments to both validate the methods of analysis and establish a baseline of results to be used for future analysis.

The first step was to collect sufficient amounts of RNA for all downstream steps. This was important since this is where RNA degradation often occurs (Wang, et al. 2008). We established that roughly 22μg of total RNA from larval CNSs was needed. Even though such a large amount of RNA was required and could have easily been isolated from the whole larvae, the idea of maintaining the same tissue type as would normally be studied has been shown to be crucial since primers may act differently in the presence of other tissue types in subsequent experiments (Wang, et al. 2008). Therefore, we first isolated total RNA from explanted CNS tissues from w^{1118} larvae. Next, we determined the concentration and integrity of our RNA using an Experion system. The results (Appendix II, Supplemental Table 2) reported both concentration and an RNA quality indicator number (RQI) for each sample. Our results indicated that samples obtained had a > 7 RQI (high quality). Following optimization of RNA isolation, we next had to determine efficiencies of our primer probes. Theoretically, a PCR reaction doubles the product each cycle; however, this assumption is based on a 100% efficient reaction. Typically a good primer probe has a range of 90-110%. We then proceeded to systematically tests all 79 of our miRNA probes along with our 3 remaining reference gene probes for efficiency. Amplification efficiency was determined for each primer set (data not shown). Unfortunately, we were not able to generate good efficiency curves for all miRNAs. This could be due to the relative low abundance of miRNAs in the CNS or repeated freeze/thaw cycles of the primer plate. The controls were tested separately in

quadruplicate and their efficiencies were determined. An example for U1 snRNA can be seen in Appendix I, Supplementary Figure 4. These results indicated low efficiency percentages for all reference genes (U1 snRNA: 63.6%, U5 snRNA: 62.0%, 185 snoRNA: 66.7%). While the exact reason was not determined, it is possible that multiple freeze/thaw cycles might have affected the integrity of reference gene primer sets. Finally, we performed melt curve analysis on the entire miRNA primer probe collection in order to judge the specificity of the primers. The results obtained from this analysis indicated that 13 miRNA primer probes, 16% of all probes, were shown to form non-specific products. All miRNA primers with bad melt curves were eliminated from analysis in subsequent experiments due to an inability for accurate quantification. A complete miRNA melt curve summary can be found in (Appendix IV). Representative melt curves depicting single product and multiple products are also shown (Appendix I, Supplemental Figure 5). It should be noted all miRNAs previously depicted as being highly regulated by activity (Figure 5) all had single primer products.

In summary, our optimization experiment successfully determined that our RNA isolation technique yields high quality RNA. Secondly, while we were not able to generate efficiencies for every miRNA primer, efficiencies for controls were collected. Finally, our results were also able to sift out any bad primer sets that may skew future results.

3.2.5 Accurate stability analysis of relative quantification RT-qPCR reference genes

The use of quantification methods in RT-qPCR provides the ability to turn cryptic cycle threshold values (C_t) into understandable results such as fold change. This can be

accomplished in one of two ways. The first method relies on inputs of known efficiency values for both unknown sample primer and a reference gene, known as the Pfaffl method (Pfaffl, 2001). This is most often referred to as the most accurate relative quantification method. The second method simply involves the use of a reference gene to standardize values and subsequent conversion to fold changes with no regard to efficiency, known as the $\Delta\Delta C_t$ or Livak method (Livak, et al. 2001). Both methods are dependent on amplification efficiencies of the reference gene(s). Since amplification efficiencies could not be determined for our unknown miRNA probes (see methods), we elected to employ the $\Delta\Delta C_t$ method for our relative quantification analysis. .

The pre-requisite for the $\Delta\Delta C_t$ method is that a reference gene, simultaneously tested with unknowns, is unaffected by the conditions that you are testing, meaning that its levels do not differ. It is for this reason the employment of reference gene stability analysis is important for obtaining accurate results. Currently four methods are commonly used to depict the overall stability of normalization controls: Delta C_t (Silver, et al. 2006), Bestkeeper (Pfaffl, et al. 2004), GeNorm (Vandesompele, et al. 2002) and Norm finder (Andersen, et al. 2004). These analysis methods determine, through statistical functions, how variable the levels of a particular reference gene are across conditions. Specifically, these analysis methods can help determine if any of our reference genes are activity-dependent, such as U12 snRNA and U76 snRNA, which was previously determined (data not shown). Unfortunately, this is a procedure that is not often utilized by many researchers, who simply assume well-known standards like GAPDH will remain stable in all conditions and samples.

Our first approach was to determine which of our reference genes still in use was the most stable. Our remaining genes following preliminary experiments and subsequent optimization were U1 snRNA, U5 snRNA and 185 snoRNA. In order to accurately determine reference stability, C_t values for each condition tested needed to be collected. Fortunately, the data required for this analysis was collected internally during the large-scale experiment described in Section 3.2.7. This provided us with a large number of internal C_t data for each reference gene under both high potassium and control conditions. Following the analysis, reference gene usage could be retroactively imposed. The results for all aforementioned analysis methods were generated on a consolidated website (Zhang, 2010) which employed all methods and generated an overall result graph. The results for all tests are reported in Appendix I, Supplementary Figure 6. Our analysis indicated that the U1 snRNA was the most stable reference gene in the larval CNS during spaced training using high potassium. In summary, using these statistical tests, they allowed us to select a single, validated reference gene for subsequent analysis.

3.2.6 Development and validation of an absolute quantification control

Our second approach was to spike RNA samples prior to reverse transcription, with a known concentration of a synthetic miRNA in order to determine absolute copy numbers of miRNAs in stimulated and un-stimulated samples. Two potential miRNAs were proposed for the spike in: human miR-559 and miR-640. These miRNAs were selected due to their lack of homologue expression in *Drosophila* and an absence in sequence complementation in the *Drosophila* transcriptome (data not shown). These synthetic miRNAs were then validated. The results determined that synthetic miR-559

had poor standard curve generation and was thrown out (data not shown). In contrast, the results for synthetic miR-640 indicated that it was a viable candidate. The C_t graph and standard curve showed even spacing and a standard curve correlation value of R^2=1.00. Efficiency of this miRNA was 96%, well within the MIQE guidelines. Finally, the miR-640 showed a strong single product signal as seen in the figure (data not shown). Together, these results indicated a validated absolute quantification control.

3.2.7 An optimized multi-replicate RT-qPCR screen of the Canton S larval CNS reveals significant differential expression of miRNAs following spaced training

Following optimization of the $\Delta\Delta C_t$ and absolute quantification methods, we wished to determine if significant differential expression of miRNA in the larval CNS following LTM-associated spaced training was occurring. For this large-scale experiment in order to examine statistical significance, 3 biological replicates of stimulated and control samples were obtained. Following high potassium spaced training, RNA isolation was performed. RNA integrity analysis was performed and the results determined that all samples had RQI >7.0 (the established minimum) (Appendix II, Supplemental Table 3). It was determined, based on U1 snRNA normalized ($\Delta\Delta C_t$ methods) results that 4 miRNAs exhibited > 2-fold reduction in levels 1 hour after final stimulation (Table 1). The two greatest differential expressions were from miR-314 and miR-958 with average fold

	Relative Quantification		Absolute Quantification	
	$\Delta\Delta C_t$ Analysis Results		Copy Number Results	
miRNA Name	U1 Norm. Average Fold Change (x)	2 Tail T-Test P Value	Average Fold Change (x)	2 Tail T-Test Value
miR-1	-3.1	0.05	-1.12	Not Tested
miR-8	-1.85	0.04	1.24	
miR-289	-2.68	0.01	-1.45	
miR-314	-7.46	0.02	-4.85	0.121
miR-958	-14.78	0.02	-6.9	0.02

Table 1-Large scale 3-biological replicate high potassium spaced training of the Canton S larval CNS reveals significant differential expression of miRNA using both relative and absolute quantification methods. This Summary table depicting both quantification methods and values pertaining to the initial miRNA identified. Relative quantification is based on a U1 snRNA reference $\Delta\Delta C_t$ method. Absolute quantification represents determination from copy numbers referenced to our synthetic miRNA miR-640 Green represents meeting or exceeding threshold, red indicates that threshold was not obtained.

changes of -7.46x and -14.78x respectively. These relative quantification results were also shown to be statistically significant with all miRNAs (Table 1). Additionally, after this analysis was performed, miR-8, although having a fold change of only -1.85x, was shown to be significant (Table 1). In terms of absolute quantification, which ran under the assumption that amplification efficiency for all unknowns was the same as the synthetic spike-in, revealed 2 miRNAs to be reduced in levels > 2-fold (Table 1). These two miRNAs, miR-314 (-4.85x) and miR-958 (-6.9x), underwent statistical analysis of copy number and found that only miR-958 was significantly down-regulated following spaced training (Table 1). These results suggested a general down-regulation in miRNA expression occurred 1 hour after spaced training occurs. These results also implicated, in both relative and absolute quantification analyses, miR-958 as being highly down-regulated following this activity induction. This novel finding had several important implications. First, to the best of our knowledge, miR-958 has not been studied in any context in *Drosophila*. Second, miR-958 is predicted to regulate several highly relevant targets. The latter will be addressed in the following chapter.

CHAPTER FOUR: *IN SILICO* ANALYSIS OF MIR-958 TARGETS IMPLICATES DLAR AS A POTENTIAL TARGET OF REGULATION

4.1 Introduction

Explorations into miRNA/mRNA interactions have primarily been based on specific sequence complementation. The most important portion of a miRNA resides in nucleotides 2-9 at the 5' end, often referred to as the "seed region". This region requires at least 7 nucleotide binding complementation in order to properly bind to the mRNA. Variations of this binding include a 2-7nt seed sequence complementation followed by an A (7mer-1A), the stronger 2-8nt seed sequence complementation (7mer-m8), and the strongest 1-8nt seed sequence complementation (8mer). One location this binding can occur is within the 3' untranslated region (3'-UTR) (Seggerson, et al. 2002). Using this specific sequence requirement, the employment of investigative computational (*in silico)* bioinformatics has emerged to provide powerful search algorithms that essentially BLAST the genome for sequence complementation. Typically these target prediction algorithms work in one of two ways. The first takes a thermodynamic approach. The likelihood of a valid target is based on free energy association of the miRNA seed region and subsequent sequence to the predicted target. Databases like RNAhybrid (Rehmsmeier, et al. 2004) exhibit this type of target identification and subsequent ranking. The second method works by comparative analysis of inter-species target sequence conservation and total binding site. This method is employed by databases like

PicTar (Grün, et al. 2005) and TargetScan (Friedman, et al. 2009; Grimson, et al. 2007; Lewis, et al. 2005). While both analysis methodologies are sound in their approach, literature suggesting that important regulatory mechanisms such as miRNA binding sites exhibit cross-genus conservation has caused researchers to gravitate towards the use of the second method. However, as is the case with most biological mechanisms, it is almost never one or the other; it is some combination of both choices. To account for this, miRecords has recently been developed (Xiao, et al. 2009). This database does not have a specific algorithm to identify miRNA/mRNA interactions but instead is a cross comparison database linker that brings together prediction results from 11 databases that each has their own specific algorithm. This powerful tool ranks miRNAs associated with a target based on how many databases they are present in. This cross-platform ranking technique is advantageous due to its ability to identify miRNA/mRNA interactions predicted independently using a variety of approaches, which may significantly strengthen its potential validity. At very least, these multiple independent predictions suggest a conserved interaction that should be investigated further.

In Chapter 4, we propose that a 3-stage process can be employed using miRecords to predict potentially relevant targets of a particular miRNA. In our previous results we have shown miR-958 to be activity-dependent down regulated in the larval CNS. Importantly, we predict that utilizing these bioinformatic tools will lead to accurate identification of miR-958 targets that control activity-dependent synaptic growth. We report that utilizing this 3-stage approach for miR-958, 13 mRNA targets implicated in processes surrounding synapse structure, synapse function or learning and memory have

been identified. Interestingly, one target in particular, the *Drosophila leukocyte-antigen-related-like* receptor tyrosine phosphatase (Dlar), is predicted to be regulated by 2 additional activity-dependent miRNAs identified in this study.

4.2 Results

The use of the following 3-stage process was employed to identify potential mRNA targets of miR-958, although it can be used for investigation of any other *Drosophila* miRNA,

4.2.1 Stage 1: Initial Scan of miRecords for possible targets of Drosophila melanogaster miR-958

An initial query of the predicted targets database section of miRecords for miR-958 revealed a combined 1,262 potential mRNA target 3'UTRs. The comparative analysis provided resource reporting from 9 of 11 databases for *Drosophila* based inquiries. The remaining two: PicTar Fly and TargetScan Fly 5.1 needed to be cross-referenced manually.

4.2.2 Stage 2: Cross-referencing the miRecords query PicTar and TargetScan Fly predictions

A query of PicTar revealed that the database does not contain predictions for miR-958 due to its dataset having been published before the discovery of this miRNA in 2007 (Grün, et al. 2005). This step was taken because the miRecords-based cross-platform reporting algorithm does not actively recruit data from this source for any *Drosophila* miRNA or mRNA target. Following this, a query of TargetScan Fly 5.1 for miR-958 targets revealed 126 potential targets that are conserved among 11 species of

Drosophila. The easiest method with these smaller result sets was to manually search and tag if present in the master miRecords target list. Once this cross-referencing was completed, the now annotated miRecords master list was sorted. First, the sum the total databases each target was determined. Next, although the annotated list contained targets present in 1-4 databases, we set our analysis cut-off for targets predicted in 3+ databases. Targets present in < 3 databases are still considered to be potentially relevant; however, we consider target mRNAs present in 3+ databases to be of a greater interest.

4.2.3 Stage 3: Systematic identification of interesting 3+ cross-platform identified targets

Following the generation of targets predicting regulation by miR-958 in 3+ databases, the biological relevance of each target was determined. This occurred by checking each identified target for certain criteria, all of which were found in *Drosophila* genetic information database FlyBase (Tweedie, et al. 2009). The primary screening criterion was that the mRNA has an annotation in FlyBase indicating a role in synapse structure, function or learning and memory. Based on this criterion, a smaller list of potential targets was generated (Table 2). The target that had the highest number of databases present was then considered. In the case of miR-958, this is the Leukocyte antigen-related like receptor tyrosine phosphatase (Dlar). Dlar is potentially relevant for two reasons. The first is that it is implicated in synapse formation and size determination, specifically that the levels of Dlar are directly proportional to synapse complexity (Kaufmann, et al. 2002). The second and arguably more intriguing reason for the importance in selection of Dlar is that it is also predicted to bind to miR-1 and miR-8 (Figure 7). All of these miRNAs, including miR-958, were determined to be significantly

Gene Name	MiRecords Database Hits
Synapse Structure and/or Function	
Leukocyte-antigen-related-like	4
Complexin	3
Dystrophin	3
Frizzled 2	3
Couch potato	3
Spinster	3
Comatose	3
Synaptogyrin	3
Sunday driver	3
Learning and Memory	
Neurofibrimin 1	4
No extended memory	4
Gilgamesh	3
cAMP-dependent protein kinase 1	3

Table 2- Putative targets of miR-958 regulation. There are 13 predicted mRNA targets of miR-958 that might regulate activity-dependent changes in synapse structure at the larval NMJ. *Drosophila* genes with an annotation in Flybase that indicate a function in the regulation of synapse structure and/or function or in some other aspect of learning and memory are identified here. The corresponding number of miRNA target prediction databases that indicate a potential interaction between miR-958 and each mRNA.

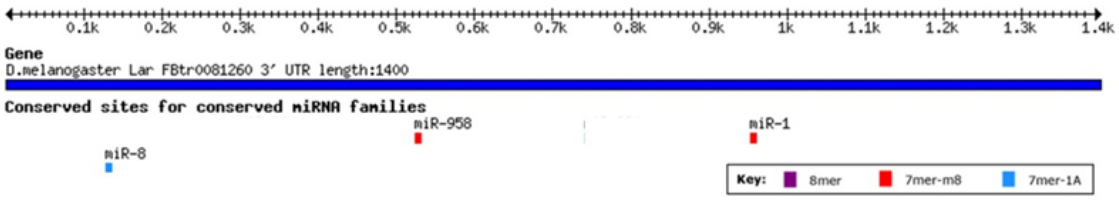

Figure 7- Dlar is predicted to be regulated by 3 identified activity-dependent miRNA. A binding diagram of the Dlar 3'-UTR showing locations for 3 activity-dependent miRNAs with seed sequence complementation. In addition, the legend associated with the types of binding is also included. Image adapted from www.targetscan.org.

down regulated by LTM-associated spaced training in the larval CNS using $\Delta\Delta C_t$ analysis (Table 1). Thus, Dlar is a putative target for 3 of the 5 activity-dependent miRNAs identified in this thesis.

CHAPTER FIVE: DISCUSSION

5.1 Summary

The work presented in this thesis has revealed several relevant results pertaining to the field of neuroscience, particularly in the *Drosophila* model system. First, the results have confirmed that a spaced training using a high potassium based stimulation paradigm was capable of inducing rapid long-lasting structural changes at the larval NMJ. In addition, miRNA microarray analysis has characterized the *Drosophila* larval CNS miRNA expression profile. Differential expression analysis of miRNAs following spaced training in the "wild-type" Canton S larval CNS has determined 5 miRNA candidates. miR-958 is of particular interest. Transcription of this miRNA was shown to be significantly down-regulated by spaced stimulation. Moreover, this miRNA, along with other activity dependent miRNA (miR-1 and miR-8) have been predicted using a novel target prediction method utilizing existing methods to possibly regulate the receptor tyrosine phosphate, Dlar.

5.2 Spaced training induction of activity-dependent changes at the larval NMJ

The development of artificial induction of synapse-associated changes relating to the formation of LTM has been important to the study of the processes underlying learning and memory. One well established method of inducing these LTM associated long-lasting changes is through the use of spaced training paradigms. Several modes of induction have been employed in these paradigms including electrical (Scharf, et al.

2002), chemical (Mauelshagen, et al. 1998; Yu, et al. 2006), behavioral conditioning (Kogan, et al. 1996) and even light (Schroll, et al. 2006). These paradigms have been demonstrated to be effective in many model systems including *Aplysia* (Mauelshagen, et al. 1998), *Drosophila* (Yu, et al. 2006; Schroll, et al. 2006) and murine models (Kogan, et al. 1996). Long-lasting structural changes have shown to be induced by spaced training paradigms in *Aplysia* and *Drosophila* (Wu, et al. 2001; Ataman et al. 2008). The ability of structural changes at the synapse to be induced by spaced training was of particular interest in our research, especially in consideration for our model synapse, the larval NMJ.

Recently (Ataman, et al. 2006) demonstrated that new synaptic growth at the NMJ can be observed by the formation of immature ghost boutons. These structures were later determined to have an activity-dependent formation using both ChR2 and high-potassium stimulation paradigms (Ataman et al. 2008). This suggests that ghost boutons are a visual example of LTM-associated synaptic growth. While our results failed to determine the ability of the transgenically expressed ChR2 selective cation channel to cause significant ghost bouton formation at the NMJ following light-induced spaced training, ghost bouton formation did indeed occur with an average increase of 2.14-fold over control (Figure 1C-D). These changes might have proved statisitically significant if the published stimulation paradigm had been followed. We had three main reasons for attempting the ChR2 approach. First, we wanted to stimulate activity in live larve using a non-invasive technique. Second, we were interested in potentially observing *de-novo* synaptic growth in live larvae *in vivo* by imaging fluorescently-labeled NMJs just under

the cuticle. Finally, the ability for the ChR2 system to cause spaced depolarizations of selectively driven motor neurons in intact larvae presents an opportunity for future studies examining the cellular and molecular processes that regulate activity-dependent in synaptic growth.

The second stimulation paradigm utilized for spaced training involved applications of a the hyperkalemic version of the HL-3 dissection buffer (Roche, et al. 2002). This paradigm, which was subsequently validated in 2 separate genotypes (w^{1118} and Canton S) provided the best results. A highly significant 5.5-fold and 6-fold induction of ghost bouton induction was observed in w^{1118} and Canton S respectively (Figures 4B & 6A). This paradigm opens an avenue of downstream research that may reveal underlying mechanisms in transcription- and translation-dependent phases of LTM formation. In particular, since LTM is a sustained process that occurs hours after stimulation, further research into this these processes may reveal key factors and regulators involved in the induction and with maintenance of long-term changes in synapse structure and/or function.

5.3 Differential expression of miRNAs in the larval CNS

LTM late-phase processes, which are both transcriptionally and translationally dependent, are of particular interest to our research. Such processes include transcriptional activation via Fos, Jun and CREB of necessary mRNAs implicated in LTM formation. Additionally, translational regulation of these and other important mRNA, such as *pumilio* have sufficiently demonstrated that the miRNA pathway is partially responsible in control of activity-dependent synaptic growth (Fiore, et al. 2009).

In an attempt determine if induction of spaced training, leads to differential expression miRNAs in *Drosophila*, it is first important to note that this has been previously explored in other model systems. The first paper (Park, et al. 2009) examined differential miRNA expression following activity induction of long term potentiation (LTP) in the mammalian murine hippocampus. Again, LTP, a process previously described in mammals, experimentally replicates synaptic plasticity based LTM formation, which is characterized by sustained increases in synaptic strength and size. A second paper published slightly after then described this same type of investigation, only in rats (Wibrand, et al. 2010). Both publications first utilized microarray analysis of miRNAs present in the organism and whereupon analyzing treated and control samples, noted differences in relative levels of miRNAs during LTP. Subsequent RT-qPCR studies essentially supported their findings that a subset of miRNAs exhibits differential expression following LTP.

Our research was conducted in a similar manner to these published works. This is stated in general terms for a reason, far more validation and optimization steps were taken in our study in an effort to generate conclusive results. The first and most notable difference in comparison was that our work was done in a highly tractable genetic model organism, *Drosophila melanogaster*. To the best of our knowledge, we present the first miRNA expression profile of the larval CNS (Appendix III). We identified 79 miRNAs, which represented a screening of 62% of known *Drosophila* miRNAs with the release of miRBase 17.0. Originally, when the array was performed, our result accounted for 99.3% coverage of known miRNAs (based on the miRBase 14.0). Utilization of the ChR2

stimulation paradigm provided an initial microarray screen of CNS-specific miRNA differential expression with >1.1-fold change (Appendix II, Supplemental Table 1B). Subsequent validation via RT-qPCR (Figure 2A) indicated conflicting results, possibly as a result of the less robust stimulation paradigm with errors in timing described above. In short, we might have missed the period of peak miRNA regulation. This idea is supported by previous studies implicating temporal expression of activity-dependent miRNAs in rat cortical neurons (Fiore, et al. 2009), which implicated this particular timeframe where differential expression begins to wane. Temporal expression analysis of these miRNAs revealed that miRNA induction peaked at 2 hours after first stimulation, and by 6 hours, basal miRNA expression was observed. This paradigm however did not involve spaced training but static "treatment" with both high potassium and BDNF containing buffers for up to 6 hours. Samples were taken from the tissue at separate time-points. While this method appears to induce activity-dependent differential miRNA expression, it does so in a chronic manner. This is different from our acute spaced training which has been shown to replicate LTM associated changes in the CNS. Nevertheless, our observations could be due to the activity-dependent miRNAs levels stabilizing following its necessary function of translational regulation, as suggested by the aforementioned publication. However, these initial miRNA microarray results did yield the novel miRNA expression profile, a highly valuable piece of information especially in neuronal development.

Subsequent analysis utilizing the high potassium based stimulation paradigm to generate differential expression of miRNAs in w^{1118} proved to be much more successful, causing activity-dependent alterations in levels > 2-fold (Figure 5). 8 miRNA were up- or

down-regulated including: miR-282, miR-314, miR-12, miR-304, miR-79, miR-8, miR-279 and miR-iab-4p. Interestingly, two clustered miRNAs, miR-304 and miR-12, appeared to be co-regulated. Joint regulation of clustered miRNAs following acute synaptic activity has been previously described by (Fiore, et al. 2009) who demonstrated that miRNAs in the miR-310 cluster undergo differential expression following stimulation with both KCl and BDNF.

However, following this experiment we decided to discontinue usage of the w^{1118} genotype for two major reasons. The first came from unpublished data from our lab, which suggested that the genotype had altered NMJ phenotypes, characterized by higher bouton numbers than other studied control genotypes. It was hypothesized that genetic modifiers acquired in the lifetime of the line may have altered synaptic growth. This was concerning due to our focus on mechanisms associated with regulating this growth. The second argument was that the miRNA microarray analysis revealed interactions between the ChR2 control sample and the w^{1118} control sample, indicating miRNAs may have been affected in this line. We decided to utilize a more wild-type line, Canton S, to establish more confident findings in future spaced-training studies examining miRNA expression.

Deviating from the mammalian studies, we chose to adhere to the MIQE guidelines in respect to RNA integrity, primer specificity, implementation of absolute quantification and reference gene validation. Our results indicated that the RNA used for subsequent RT-qPCR studies was of a sufficient caliber, with RQI >7 in all cases. Additionally, determination of primer probe specificity to eliminate non-specific product

forming probes, guaranteed an elimination of skewed results from this type of unoptimized assay. The second major component of optimization involved data quantification. For our final statistic-generating RT-qPCR study we incorporated the use of the synthetic human miRNA miR-640. This spike-in standard allowed accurate quantification of copy number (summarized in Table 1). This method was not employed in either mammalian study and allowed us an extra level of confidence in our results. The final optimization step involved accurate determination of reference gene stability, which was important for accurate $\Delta\Delta C_t$ analysis. If the reference gene used for normalization is activity-dependent, all results may be skewed and reveal false-positives in findings. Through 4 separate tests using data from a large scale 3 biological replicate high potassium stimulation of "wild-type" Canton S revealed a noticeable difference in reference gene stability (Appendix I, Supplemental Figure 6). Our findings validated the U1 snRNA as having expression levels that were activity-independent in the larval CNS. These procedures and subsequent findings constitute a necessary step in any RT-qPCR study, especially when addressing conditional differences.

Following optimization, a large-scale high potassium-based RT-qPCR study was performed using the Canton S genotype. These results, representative of 3 biological replicates, allowed generation of statistical significance for both relative and absolute quantification methods (Table 1). One surprising find was that differential induction of all potentially relevant miRNAs (showing > 2-fold regulation) in this study occurred in a negative direction. Presumably, a decrease in miRNA levels would lead to an increase in translation of target mRNAs. This idea of general de-repression is consistent with the

notion that processes associated with LTM require new protein synthesis. Our end result suggests that 1 miRNA, miR-958, is significantly down regulated by activity when analyzed by both quantification methods. This particular miRNA underwent a relative differential expression of -14.78-fold change ($\Delta\Delta C_t$) and a -6.9-fold change (absolute quantification) in copy number, both results showing statistical significance. This miRNA has never been studied in any context and represents a novel finding that allows for a first go at characterization and analysis. *In silico* analysis implicates miR-958, along with some of the other activity-controlled miRNAs, as potential regulators of several proteins with well-characterized functions in the control of synaptic plasticity.

5.4 Identification of target mRNAs for activity-dependent miRNAs

Activity-dependent translational regulation at the synapse of these proteins has been shown to be regulated by miRNAs. One example of this is miR-134 regulation of LimK1 kinase expression in mammalian dendrites (Schratt, et al. 2006). Upstream activity-dependent signaling cascades involving transcription factors such as Fos, Jun and CREB then work to initially activate the transcription of components necessary to maintain these initial changes. For instance, activity-dependent CREB was shown to activate miR-132 which leads to repression of the Rho associated p250GAP GTPase leading to sustained dendritic growth (Wayman, et al. 2008). Homeostatic regulation of mRNAs required for these lasting changes such as *pumilio* have been shown to temporally regulate by miRNAs, specifically a cluster of miRNAs (Fiore, et al. 2009). Taken together these findings suggest a precedent for activity-dependent mRNA

regulation by miRNAs as being a likely candidate for acting as regulators of synaptic plasticity.

The results of this thesis demonstrate that the activity-dependent miRNA, miR-958, is a predicted regulator of 13 mRNA transcripts whose protein products are required for long-lasting changes at the synapse similar to those associated with LTM. These results were determined using miRecords, in combination with the PicTar and TargetScan Fly 5.1 miRNA target prediction databases. Screening of these results has implicated one mRNA, encoding for Dlar, as a pertinent LTM relevant protein that is associated with synapse formation. This receptor tyrosine phosphatase has been shown to interact with liprin-α to control synapse complexity in *Drosophila* (Kaufmann, et al. 2002). It was also shown is this paper that synapse complexity is highly sensitive to Dlar levels. The reduction of Dlar by roughly 50% in mutant flies resulted in half the synapse complexity at the NMJ when compared to controls. This knowledge that Dlar levels correlate directly to complexity further justify our interest in the study of its regulation. In this regard, we discovered that in addition to miR-958 Dlar is predicted to be a target for 2 other activity dependent miRNAs: miR-1 and miR-8 (Figure 7). Taken together, we expect the potential of Dlar to be a subject of interest in the LTM associated activity-dependent process of sustained structural changes at the synapse to be quite likely. However, subsequent miRNA-target validation needs be performed before further conclusions can be drawn.

5.5 Future directions

With the completion of this research, it becomes clear that many future projects must be undertaken. First, the validation of Dlar regulation by miR-958, miR-1 and miR-8 must be performed. This will be done using a validated method involving *in-vitro* plasmid-based reporter constructs in *Drosophila* Schneider 2 cells. Second, generation of transgenic fly lines both for miR-958 over-expression as well as miRNA sponge-based miR-958 knockdown (Ebert, et al. 2010) will be generated for functional analysis at the larval NMJ. For example, we suspect that if miR-958 is essential for rapid activity-dependent ghost bouton formation following spaced stimulation, then miR-958 over-expression in motor neurons may significantly reduce new bouton growth. Third, fly lines can also be obtained for over-expression and knockdown for Dlar to determine if ghost bouton formation following activity is altered, which would support the hypothesis that this protein is required for these LTM associated changes. Fourth, another study that should be performed to determine the temporal expression of our 5 identified activity-dependent miRNAs. This experiment, similar to the one presented in (Fiore, et al. 2009), will allow us to identify peak levels of regulation and to determine if miRNA return to basal levels following their differential expression. Finally, in a more general sense, the beauty of this project is that it has generated a list of 5 total miRNAs that are differentially expressed, each having several relevant mRNA targets relating to synaptic growth. The opportunity for hundreds of future target validation and functional analysis studies would be able to draw their basis from work generated in this project. In

summation, based on these data generated from this thesis, there are more directions that can be taken that can even be currently presented.

CHAPTER SIX: METHODS

6.1 Fly Strains

Strains used in this project were: w^{1118}, Canton S, C380-Gal4 and UAS-ChR2 (II, III). Unless otherwise indicated, all strains were raised on normal Bloomington food. All strains and crosses were kept in diurnal incubators at 25°C with 70% ambient humidity.

6.2 ChannelRhodopsin-2 (ChR2) rapid-activity stimulation

6.2.1 Construction of the ChR2 stimulation apparatus

The ChR2 stimulation apparatus was conceived, designed and built based on previous descriptions (Schroll, et al. 2006; Ataman, et al. 2008). The apparatus's primary purpose was to effectively activate light-gated cation channels that were selectively expressed in motor neurons. A 1-square foot acrylic cutout was used as a base for the electronics and stimulation chamber. The electronics included two wiring distribution blocks as well as a reed relay, which was used to trigger DC current when an input signal was received. The chamber, a 2-inch inner diameter 6-inch long acrylic tube, was hinged onto a bored depression in the base the exact diameter of the agarose stimulation plates used. In this same depression a smaller hole was made to hold one of the two Luxeon V star light emitting diodes (LED) (Luxeon Inc.). This provided ample 470-nanometer light (activation wavelength for ChR2) from the underside of the dissection dish. A solid acrylic cylinder wedged in the top of the acrylic tube provided a mount for the second LED. This LED included an accessory parabolic (PAR)-type projector lens (Luxeon Inc.)

which allowed for proper overhead light dispersion. This chamber assembly served two purposes: proper alignment of the LEDs, and to sandwich the two parts of the plate to create a self-contained environment so the larvae could not escape. The agarose stimulation plate itself was inlaid with a segment of a 15ml conical tube and was filled with a 2% agarose solution. Aside from the main stimulation apparatus, a constant current DC power supply (EXTEC ®) and a pulse stimulator (A-M Systems ™) were used in conjunction for proper operation. The DC power supply was used to provide a constant 700mA to each LED. The pulse stimulator, programmed to provide the proper pulse rate in each stimulation step was used to trigger the reed relay, allowing current to flow and activate the LEDs.

6.2.2 ChR2 stimulation paradigm

12-15 non-wandering 3rd instar transgenic larvae, constructed by crossing UAS-ChR2 (II, III) male flies (Schroll, et al. 2006) with C380-GAL4 (Budnik, et al. 1996) female virgins, were extracted from modified fly food. Bloomington food was supplemented with 100mM all-trans retinal to ensure proper operation of the ChR2 cation channel (Nagel, et al. 2002; Schroll, et al. 2006). Following extraction, the larvae were washed twice in pH=7.3 haemolymph-like (HL-3) dissection buffer (Stewart, et al. 1994). A maximum of 11 intact larvae were then placed within the conical tube cutout on the agarose stimulation plate and then sealed with the opposite side of the dish. The plate was then loaded in the stimulation apparatus chamber and hinged shut. Spaced training via light induced motor-neuron depolarization was then performed. The rapid-activity spaced training stimulation paradigm was a slightly modified version of that described in

(Ataman, et al. 2008). The paradigm utilized 5x 5-minute stimulation steps, with each step encompassing a 2 second on 3 second off LED cycle. These stimulation steps were separated by 15-minute rest periods. Following the final stimulation step, a resting period of 134 minutes occurred. Upon completion of the stimulation paradigm larval preparations were either fixed for immunohistochemical studies or underwent CNS microdissection for RNA isolation. Un-stimulated controls were obtained in the same manner as above except the DC power supply was left off.

6.3 High Potassium perfusion-based stimulation

6.3.1 Construction of the high potassium stimulation apparatus

This stimulation apparatus was constructed to provide a cost-effective multi-plate tabletop perfusion platform utilized for the application of high potassium dissection buffers onto semi-intact *Drosophila* larvae. Construction began by altering a pre-formed weighted acrylic base (World Precision Instruments). This base, equipped with threaded holes, was modified by creating two depressions with the exact diameter as our dissection plates. Flat magnetic runners were then placed on both sides of the depression cutouts to hold magnetic tube holders. For a dual buffer delivery system, a variable height dual 60ml syringe holder was affixed to a 3 foot length of threaded steel rod, which was then attached to the threaded hole in the weighted base. This setup allowed for a gravity-fed buffer delivery system. Using Tygon® tubing, two inline manifolds, four variable flow valves and two clipped and shaped 14Ga needles affixed to two magnetic tubing holders, specific dissection buffers could be delivered to both dissection plates simultaneously at controlled rates. To make this a true perfusion system, a vacuum system to effectively

evacuate the buffer from the dissection plate had to be incorporated. The first step involved creating a 5mm cutout on the outer edge of the sylgard polymer which lined the dissection plates to allow for proper buffer pooling. For each dissection plate, a pre-made angled vacuum nozzle attached to a magnetic tubing holder was placed in the sylgard cutout to create an avenue of buffer removal. These vacuum nozzles were then linked to a manifold, which provided equal vacuum pressure to each plate. This manifold was then connected to a vacuum flask. The flask was then joined to a variable pressure vacuum pump on a pedal control circuit.

6.3.2 High potassium stimulation

The buffers used were pH=7.2 adjusted normal 5mM KCl HL-3 (Stewart, et al. 1994) and 90mM KCl HL-3 (Roche, et al. 2002). The High K^+ HL-3 was adjusted for osmolarity changes (in mM; 40 NaCl, 90 KCl, 20 $MgCl_2$-$6H_2O$, 1.5 $CaCl_2$, 10 $NaHCO_3$, 5 Sucrose, 5 Trehalose, 5 HEPES). Osmolarity testing was performed on a μOsmette Osmometer (Precision Systems, Inc.). Then, depending on the experiment, either w^{1118} or Canton S fly strains were used. 20-40 non-wandering 3rd instar larvae were removed from fly food and washed twice in the 5mM KCl HL-3. Following this, up to 20 unstretched larvae were pinned perpendicular to the buffer flow on each modified sylgard dissection plate. An anterior-posterior transverse incision was made in each larva and the bodies were partially cleaned, leaving the CNS intact. The plates were then loaded on to the perfusion system's base. 60ml perfusion volumes of the 5mM and 90mM KCl HL-3 solutions were used for rest and stimulation steps respectfully. The KCl-based spaced training paradigm utilized 2, 2, 2, 4 and 6-minute stimulation pulses each separated by 15

minute rest steps. After the final stimulation step, a rest period of 74 minutes occurred. Upon completion of the stimulation paradigm, larval preparations were either fixed for immunohistochemical studies or underwent CNS microdissection for RNA isolation. Un-stimulated control samples were obtained in the same manner except during perfusion; the 5mM KCl HL-3 replaced the 90mM KCl HL-3 during the stimulation steps.

6.4 Immunohistochemistry

Larval preparations were fixed in 3.5% paraformaldehyde for 20 minutes in PBS buffer (pH=7.2). After washing in PBS and PBS with 1% Triton X-100, preparations were blocked for 30 minutes in Block solution (PBS containing 0.1% Triton X-100, 2% BSA and 5% normal goat serum). Primary antibodies used were mouse anti-DLG (Developmental Studies Hybridoma Bank) and goat anti-HRP conjugated to Dylight 594 (Jackson Labs). The concentrations for these antibodies were 1:500 and 1:100 respectively. The secondary antibody used was anti-mouse IgG conjugated to Alexa 488 (Molecular Probes) at a concentration of 1:100. Labeled preparations were then mounted on double frost glass slides in Vectashield (Vector Labs) mounting media containing DAPI and stored in the dark at -20°C prior to imaging.

6.5 Imaging of ghost boutons

Imaging of larval NMJs was performed on an Olympus FluoView FV1000 scanning confocal microscope. With the exception of NMJs from the Canton S ghost bouton study, which utilized a 100x objective (N.A. 1.4), all other imaging studies employed a 60x (N.A. 1.35) objective. All NMJs were located in larval abdominal section 3 on muscles 6/7. Z-stacks were obtained at 0.8 μm intervals that were combined

by the FV1000 imaging software. Determination of valid ghost boutons was outlined by previous methods in (Ataman, et al. 2008). Bouton structures, showing presynaptic HRP reactivity but lacking postsynaptic DLG association were identified. These structures > 1μm in size were considered a valid ghost bouton. In all reported results, n was equal to the number of NMJs imaged with error determined by +/- SEM.

6.6 RNA isolation from the larval CNS

CNS samples were obtained from stimulated and un-stimulated larvae following the final rest step in either ChR2 or High K^+ stimulation paradigms. All extraneous tissue (imaginal discs, etc.) was dissected away leaving just the optic lobes and ventral ganglion. Generally speaking, each isolation required a total of 30-50 CNS samples. All RNA work was done in a dedicated RNA hood. Using a TissueRuptor (Qiagen) the CNS tissues were homogenized in the provided lysis solution (Exiqon A/S). Following homogenization, total RNA was isolated from CNS samples using the spin column-based miRCURY ™ RNA isolation kit (Exiqon A/S). A single elution with a volume of 50μl was obtained. Except for the initial w^{1118} RT-qPCR isolation, following this, a 4μl aliquot of the elution was placed in to a 0.6ml micro-centrifuge tube for downstream RNA integrity analysis. Both tubes were then snap-frozen in liquid nitrogen and stored at -80°C.

6.7 Determination of RNA concentration and integrity

Accurate concentration and integrity of isolated RNA is paramount to successful downstream applications such as RT-qPCR. For this reason we employed the use of the use of the Experion automated electrophoresis system (Bio-Rad). It was determined that

the RNA stdsense kit (Bio-Rad), with its 10ng-500ng/µl detection range, was best suited for our samples. The system worked in a time-dependent electrophoretic manner coupled with fluorescence quantification. Specifically, electrophoretic separation of bands based on size was collected by examining the time it took to reach the detector and the relative florescence each band emitted. The generation of a florescence vs. time electropherogram and corresponding virtual gel allowed for proper analysis of concentration and integrity. Concentration of a sample was determined by the integral of the complete electropherogram. This value was then compared to an internal control reference peak area that had a known concentration. RNA integrity analysis for each sample was determined from a ratio metric calculation from integrals of the 18s rRNA and 28s rRNA peak areas on the generated electropherogram. Peak identification was accurately determined with the use of an internal reference ladder provided with the kit allowed for accurate peak alignment and identification. Following a run this calculation returned a number between 0 and 10, deemed the RNA quality indicator (RQI) (Bio-Rad). The threshold for acceptable quality RNA was set at RQI >7. All samples were at least run in duplicate. To prevent multiple freeze-thaw cycles of the isolated RNA sample, a 4µl aliquot was prepared specifically for this analysis. Following the protocol exactly, 1µl of the RNA elution was used for each replicate sample.

6.8 miRNA microarray assay

In order to determine the microRNA (miRNA) expression profile of the *Drosophila* larval CNS a commercially available miRNA microarray (Exiqon A/S) was utilized. This microarray employed a chip-based hybridization assay utilizing several

technical replicates for each genotype tested. A total of 2 genotypes with 3 conditions were tested: stimulated ChR2 transgenic larvae, un-stimulated ChR2 transgenic larvae and w^{1118} larvae serving as a second control group. The incorporation of the two ChR2 conditions acted as a first run in a screen for potential miRNAs that underwent differential expression following acute synaptic stimulation. Approximately 60 CNSs from each sample were collected and underwent RNA isolation. Total RNA concentration was determined using a NanoDrop ND-1000 spectrophotometer (Thermo Fisher Scientific, Inc.) and RNA integrity analysis was performed by Exiqon after samples were shipped to their location. Their integrity analysis indicated that the quality of our samples were below what they recommend for miRNA analysis, however, this depends on the sample tissue type. At the time of the assay, the current *Drosophila* miRNA microarray chip in use was based on miRBase 14.0 (Griffiths, et al. 2004; Griffiths, et al. 2006; Griffiths, et al. 2008; Kozomara, et al. 2011). This version contained only 148 annotated miRNA, providing 62% coverage when compared to the current miRBase 17.0. The assay involved first labeling each sample with both Hy-3 and Hy-5 flourophores. Following this, a portion of each sample was hybridized to the *Drosophila* LNA miRNA micro-array chip and Hy-3 levels for each miRNA were collected. The other portion from each sample was pooled together and run on a separate chip where Hy-5 levels for each miRNA were collected. The Hy-5 values were used for a pooled background value. Data analysis performed by Exiqon calculated log median ratios of each miRNA for each sample. These calculations were then further refined to generate fold changes when compared to other samples in a similar manner to the $\Delta\Delta C_t$

method, except with the use of log median ratios (array specific Hy-5 normalized florescence values) rather than ΔC_t values (normalized raw C_t values generated in RT-qPCR runs).

6.9 General RT-qPCR

To more accurately investigate differential expression of the neuronally expressed miRNAs in *Drosophila,* the use of two–step quantitative real time PCR (RT-qPCR) was employed. Specifically, utilization of the 3 component SYBR® Green based miScript miRNA RT-qPCR detection system (Qiagen) was used for all RT-qPCR studies. Total RNA was first converted to cDNA using the miScript reverse transcriptase kit component. The second component of the miScript detection system, the miScript SYBR® Green PCR kit, was an all-encompassing master mix that would allow for proper amplification and detection of miRNA. This component contained a universal primer, which was previously bound to all miRNA converted in the cDNA synthesis reaction. The final component, the miScript miRNA primer assay was a mature miRNA specific primer probe, which allowed for specific detection of a particular miRNA. These primer assays were either obtained in individually or in a custom layout multi-primer 96-well plate. In addition, normalization control primer assays were also obtained from Qiagen to facilitate in proper data analysis. The controls first used in the ChR2 RT-qPCR array validation were U12 and U76. This list was expanded following the validation experiment to: U1 snRNA, U5 snRNA, U12 snRNA, U76 snRNA and 185 snoRNA. Together these primers, in combination with the universal primer previously described, allowed for proper amplification of a double stranded specific miRNA and normalization

control amplicon. This amplicon in turn could then be detected by the SYBR-1® flourophore present in the real time reaction, as it would non-specifically bind to double stranded DNA products. Reaction setup for all experiments utilized a 0.5µl cDNA input. All RT-qPCR assays were performed using an ICycler thermocycler (Bio-Rad) equipped with the IQ5 real-time PCR detection system hood (Bio-Rad) and controlled by the IQ5 optical system software v1.2.

6.10 RT-qPCR for miRNA microarray validation

Based on the miRNA microarray results (Exiqon A/S), 22 miScript primer assays (Qiagen) were acquired. These primers were used to probe for the miRNAs that exhibited differential expression of > 1.1x from the ChR2 stimulated and un-stimulated samples. At the time, miScript primer assays were unavailable for miR-14 and therefore was excluded from this study. In addition, a mistake was made in ordering miR-10 since miR10* was the intended target. As such, miR-10* was not quantified. ChR2 genotype stimulated and control samples were treated with light-induced spaced training manner previously described. Each sample had a starting input of 40 CNSs. A single biological replicate was tested in this study. RNA isolation was performed in the manner previously described, with the exception of not creating a 4µl aliquot. RNA concentration was determined using the ND-1000 NanoDrop (Thermo Fisher Scientific). cDNA synthesis of each treatment group then occurred utilizing 6.2µg and 6.8µg total RNA input from control and stimulated groups respectively. Reaction setup and execution were performed in the same manner previously described utilizing 3 technical replicates for each sample. Results were normalized to U12 snRNA and U76 snRNA.

6.11 Initial high potassium stimulation miRNA RT-qPCR Screen

For this experiment the w^{1118} genotype was used. Stimulated and control samples were treated using high potassium spaced stimulation in the manner previously described. Each sample contained 30 CNSs and represented a single biological replicate. RNA isolation of the CNS samples was performed in the manner previously described. Following isolation, RNA concentration and integrity analysis were performed with the Experion system (Bio-Rad) in the manner previously described. Once the samples were deemed acceptable (RQI > 7), cDNA synthesis occurred using 6µg and 7µg total RNA input for stimulated and control groups respectfully. For this experiment every miRNA in the larval CNS miRNA expression profile (79) were under investigation. As such, this experiment utilized the custom made 96-well miScript primer assay plate (Qiagen). All 5 previously described normalization controls were present on this plate in a standardized format. In addition, a negative control was also included on the plate. Reaction setup was performed in the method previously described utilizing 3 technical replicates per treatment group with 1 plate per technical replicate. Pre-programming of the IQ5 optical system software (Bio-Rad) with annotated replicate plates was also performed. This step ensured well and treatment group identification for a more organized dataset. Real-time PCR was then performed in the manner previously described.

6.12 miRNA RT-qPCR Optimization

6.12.1 miScript Primer Efficiencies and Melt Curve Analysis

In order to determine amplification efficiencies, 22µg of RNA was obtained from 120 w^{1118} larval CNSs in three separate isolations. All three samples underwent RNA

integrity analysis using the Experion system. The samples achieved RQI > 8, and were subsequently reverse transcribed. Following this, primer efficiencies plates were designed and programmed into the IQ5 software. Each column of the master miScript primer assay plate (Qiagen) was tested on 1 plate in which a duplicate 6-step serial dilution 1e-1 to 1e-6 of input cDNA was made to create a standard curve of each primer. Addition of a melt curve analysis step was added to the IQ5 protocol to determine primer specificity. General reaction setup, except for the input cDNA amounts, was performed as previously described. After the run completed, generation of standard curve and first derivative melt peak graphs for each primer tested occurred. This process was repeated until column 7 of the primer plate when it was determined that reaction efficiencies for miRNA primer probes were unable to be generated, due an inability to detect product in more dilute cDNA samples. It was decided to just run column 11 (controls) in an effort to determine efficiency and specificity. A repeat of the control analysis followed in which a quadruplicate 6-step serial dilution series was used to attain higher R^2 values on the standard curve.

6.12.2 Determination of control housekeeping gene stability

Three normalization control genes, U1 snRNA, U5 snRNA and 185sno RNA, required stability analysis to determine if levels changed following spaced training. This essential step, required for validation of a normalization control, was performed using 4 statistical-based tests. The result of these tests would reveal a ranking of stability from input raw C_t values for each control across 18 replicate studies (3 biological 3 technical per biological per condition) effectively analyzing results from treated and control

samples. These data were collected from the large scale Canton S RT-qPCR study. The Delta Ct (Silver, et al. 2006) relied on ranking by way of the standard deviation for each control, with a lower value indicating higher stability. BestKeeper analysis (Pfaffl, et al. 2004) centered on the Pearson correlation coefficient of the input data from each control to affix stability ranking values. NormFinder (Andersen, et al. 2004) analysis incorporated the use of a proprietary "stability value" from its statistical tests in stability determination. Finally, GeNorm (Vandesompele, et al. 2002) analysis also incorporated a proprietary stability value for gene stability ranking. This analysis was performed at a central website (Zhang, 2010) that allowed simultaneous testing of all 4 tests on all 3 controls. The website also produced a general ranking graph that took results for all 4 tests and ranked by majority.

6.12.3 Generation of synthetic miRNA spike-in for absolute quantification

An initial investigation into miRBase determined that several miRNA in *Drosophila* do not have homologues in *Homo sapiens*. As such, 2 miRNAs: hsa-miR-559 and hsa-miR-640 were selected due to lack of complementation with the *Drosophila* transcriptome. Synthesis of these 21nt ssRNA oligonucleotides was performed by Integrated DNA technologies (IDT), with an extra RNAse-free HPLC treatment to ensure RNA integrity. Reconstitution of each miRNA resulted in stock solutions of 4e12 copies/µl. Leftover RNA from the previous efficiency analysis was spiked with both synthetic miRNA to a final cDNA concentration 1E12 copies/µl. From here efficiency and specificity analysis was performed in triplicate 6-step serial dilutions for each synthetic miRNA. miScript primer assays (Qiagen) targeted to both miRNAs were used.

Although melt curve specificity analysis revealed single products for both miRNAs, the generated standard curve of hsa-miR-559 showed a lower R^2 value of 0.992 than the hsa-miR-640 R^2 value of 1.00. As such, we selected hsa-miR-640 for our validated synthetic miRNA spike in control for absolute quantification.

6.13 Large-scale high potassium stimulation miRNA RT-qPCR study

Following optimization of our RT-qPCR assay, a large-scale study was performed. 3 separate RNA isolations from 30-40 5x high potassium stimulated 3rd instar larvae Canton S CNSs. This was then repeated for controls. Together, this constituted a 3 biological replicate study. RNA concentration and integrity analysis was then performed in duplicate for each RNA isolation (Appendix II, Supplemental Table 3). Each sample received RQIs > 7.5 and was deemed acceptable. The reverse transcription reaction for each sample was set to an input of 6,500ng of total RNA. In addition, sufficient hsa-miR-640 synthetic miRNA spike-in was added to generate a 1E9 copies/µl cDNA. Following the RT reaction, a master run primer plate (Qiagen) was designed that encompassed all 79 miRNAs from the original miScript primer plate. In addition, the U1 snRNA, U5 snRNA and 185 snoRNA normalization controls primers were included. Finally, a duplicate 7-step dilution series for hsa-miR-640 was incorporated. This master primer plate, containing enough primer volume for all plates, was subsequently aliquoted to 18 individual plates which then were sealed with microseal F-foil (Bio-Rad) to prevent evaporation during storage at -20°C. This technique prevented repeated freeze/thaw of the primers. For each plate, the use of a single primer plate was required. Each plate required the use of two master mixes, a 90-reaction set with cDNA included, and an 18-

reaction set for the spike-in dilution series. The latter set did not include cDNA but instead was inputted in a separate dilution series corresponding to 1E9 to 1E3 copies/µl of the synthetic miRNA miR-640. Each biological replicate was run in technical triplicate, constituting 9 plates per condition. Following completion of the experiment, results were quantified.

6.14 Data Normalization

6.14.1 Relative Quantification

Analysis of differential fold change based on C_t results was performed with the $\Delta\Delta C_t$ (Livak) method (Livak, et al. 2001). Normalization controls used were U1 snRNA, U5 snRNA, U12 snRNA, U76 snRNA and 185 snoRNA. In the ChR2 RT-qPCR study, only U12 snRNA and U76 snRNA were incorporated for normalization. All 5 of the controls were used for normalization in the w^{1118} high potassium RT-qPCR study. The final Canton S experiment utilized the U1 snRNA for normalization. In all experiments incorporating normalization controls, a custom database was created to calculate ΔC_t and subsequent $\Delta\Delta C_t$ values followed by fold change values determined by the equation $2^{-(\Delta\Delta Ct)}$. This analysis assumed that efficiency of both unknown and reference primers were 100%. In the large-scale Canton S study, control $\Delta\Delta C_t$ values were pooled and compared to each of the averaged (from technical replicates) biological replicates to generate 3 separate fold change values for each normalization control. This allowed the use of statistical analysis. The use of a 2-tail unpaired student t-test assuming equal variance was employed for this analysis. The significance cut off was set to p=0.05 for all tests. Additionally a 1-factor ANOVA statistical test was also employed.

6.14.2 Absolute Quantification

This method, only incorporated with the large-scale 3 biological replicate Canton S RT-qPCR study, involved a ratio metric determination of absolute copy number between control and stimulated samples. Copy number was determined when the IQ5 software utilized the standard curve of C_t value vs. Copy number graph to match each sample with an appropriate copy number value. Similar to the relative quantification method, each control averaged biological replicate (average of 3 technical replicates) was pooled and compared to the averaged stimulated biological replicates. All of these calculations were performed in the same Excel-based custom-made database as the relative quantification calculations. This generated 3 ratios of fold change in copy number for each miRNA being tested. Again, the use of a 2-tailed unpaired student t-test assuming equal variance was employed for statistical analysis, with a significance cut-off value of $p=0.05$ having been set.

6.15 Investigative bioinformatics of miRNA-mRNA target interactions

The process involving the identification of relevant miRNA-mRNA target interaction was described in detail in chapter 4. The use of miRecords in conjunction with PicTar Fly and TargetScan Fly 5.1 provided the reference databases used for comparison. A cut-off of targets present in 3+ databases was used since these targets were denoted as a more relevant set. The use of FlyBase for relevant target determination followed the initial determination of predicted regulation. Incorporation and cross-referencing of all data was performed in an Excel-based database custom tailored to separate total databases for each relevant target.

REFERENCES

Aakalu, Girish, W Bryan Smith, Nhien Nguyen, Changan Jiang, and Erin M Schuman. "Dynamic Visualization of Local Protein Synthesis in Hippocampal Neurons." *Neuron* 30 (2001): 489-502.

Andersen, C L, J L Jensen, and T F Orntoft. "Normalization of real-time quantitative reverse transcription-PCR data: a model-based variance estimation approach to identify genes suited for normalization, applied to bladder and colon cancer data sets." *Cancer Research*, 2004: 5245-5250.

Ashraf, S I, and S Kunes. "A trace of silence: memory and microRNA at the synapse." *Current Opinion in Neurobiology*, 2006: 535-539.

Ashraf, Shovon I, Anna L McLoon, Sarah M Sclarsic, and Sam Kunes. "Synaptic Protein Synthesis Associated with Memory Is Regulated by the RISC Pathway in Drosophila." *Cell* 124 (January 2006): 191-205.

Ataman, Bulent, et al. "Nuclear trafficking of Drosophila Frizzled-2 during synapse development requires the PDZ protein dGRIP." *Proceedings of the National Academy of Sciences* 103, no. 20 (May 2006): 7841-7846.

Ataman, Bulent, et al. "Rapid Activity-Dependent Modifications in Synaptic Structure and Function Require Bidirectional Wnt Signaling." *Neuron*, March 2008: 705-718.

Baddeley, Alan D. "The influence of acoustic and semantic similarity on long term memory for word sequences." *The Quarterly Journal of Experimental Psychology*, 1966: 302-309.

Baddeley, Alan D, Neil Thomson, and Mary Buchhanan. "Word Length and the Structure of Short-Term Memory." *Journal of Verbal Learning and Verbal Behavior*, 1975: 575-589.

Bailey, Craig H, and Eric R Kandel. "Structural Changes Accompanying Memory Storage." *Annual Review of Physiology* 55 (1993): 397-426.

Bailey, H Craig, Eric R Kandel, and Kausik Si. "The Persistence of Long-Term Memory: A Molecular Approach to Self-Sustaining Changes in Learning-Induced Synaptic Growth." *Neuron* 44 (September 2004): 49-57.

Barco, Angel, Craig H Bailey, and Eric R Kandel. "Common molecular mechanisms in explicit and implicit memory." *Journal of Neurochemistry*, 2006: 1520-1533.

Benito, E, and A Barco. "CREB's control of intrinsic and synaptic plasticity: implications for CREB-dependent memory models." *Trends in Neurosciences*, 2010: 230-240.

Berdnik, Daniela, Audrey P Fan, Christopher J Potter, and Liqun Luo. "MicroRNA Processing Pathway Regulates Olfactory Neuron Morphogenesis." *Current Biology* 18 (November 2008): 1754-1759.

Bliss, T. "Synaptic plasticity in the hippocampus." *Trends in Neuroscience*, 1979: 42-45.

Brand, A H, and H Perrimon. "Targeted gene-expression as a means of altering cell fates and generating dominant phenotypes." *Development* 118, no. 2 (June 1993): 401-415.

Budnik, V, et al. "Regulation of synapse structure and function by the Drosophila tumor suppressor gene dlg." *Neuron* 17 (1996): 627-640.

Bustin, Stephen A. "Why the need for qPCR publication guidelines?-The case for MIQE." *Methods* 50 (2010): 217-226.

Bustin, Stephen A, et al. "The MIQE Guidelines: Minimum Information for Publication of Quantitative Real-Time PCR Experiments." *Clinical Chemistry* 55, no. 4 (2009): 611-622.

Ceman, Stephanie, and Julie Saugstad. "MicroRNAs: Meta-controllers of gene expression in synaptic activity emerge as genetic and diagnostic markers of human disease." *Pharmacology & Therapeutics* 130 (2011): 26-37.

Chen, Caifu, et al. "Real-time quantification of microRNAs by stem-loop RT-PCR." *Nucleic Acids Research* 33, no. 20 (2005): e179.

Chklovskii, D B, B W Mel, and K Svoboda. "Cortical rewiring and information storage." *Nature* 431 (October 2004): 782-788.

Cook, H A, B S Koppetsch, J Wu, and W E Theukauf. "The Drosophila SDE3 homolog armitage is required for oskar mRNA silencing and embryonic axis specification." *Cell* 116 (2004): 817-829.

Davis, Hasker P, and Larry R Squire. "Protein Synthesis and Memory: A Review." *Psychological Bulletin* 96, no. 3 (1984): 518-559.

Denli, A M, B B.J. Tops, R H.A. Plasterk, R F Ketting, and G J Hannon. "Processing of primary microRNAs by the Microprocessor complex." *Nature*, 2004: 231-235.

Ebert, M, and P Sharp. "MicroRNA sponges: Progress and possibilities." RNA 16, no. 11 (2010): 2043-2050.

Esquela-Kerscher, A, and F J Slack. "Oncomirs - microRNAs with a role in cancer." *Nature Reviews in Cancer*, 2006: 259-269.

Fabian, M, N Sonenberg, and W Filipowicz. "Regulation of mRNA Translation and Stability by microRNAs." Annual Review of Biochemistry 79 (2010): 351-379.

Fiore, Roberto, et al. "Mef2-mediated transcription of the miR379-410 cluster regulates activity-dependent dendritogenesis by fine-tuning Pumilio2 protein levels." *The EMBO Journal* 28 (2009): 697-710.

Frey, U, M Krug, K Reymann, and H Matthies. "Anisomycin, an inhibitor of protein synthesis, blocks late phases of LTP phenomena in the hippocampal CA1 region in vitro." *Brain Research*, 1988: 57-65.

Frey, U, S Frey, F Schollmeir, and M Krug. "Influence of actinomycin D, a RNA synthesis inhibitor, on long-term potentiation in rat hippocampal neurons in vivo and in vitro." *Journal of Physiology*, 1996: 703-711.

Friedman, Robin C, Kyle Kai-How Farh, Christopher B Burge, and David P Bartel. "Most mammalian mRNAs are conserved targets of microRNAs." *Genome Research* 19 (2009): 92-105.

Griffith, L C, L M Verselis, K M Aitken, C P Kyriacou, W Danho, and R J Greenspan. "Inhibition of calcium/calmodulin-dependent protein kinase in Drosophila disrupts behavioral plasticity." *Neuron* 10 (1993): 501-509.

Griffiths-Jones, S. "The microRNA Registry." *Nucleic Acids Research* 32, no. (Database Issue) (2004): D109-D111.

Griffiths-Jones, S, H K Saint, S van Dongen, and A J Enright. "miRBase: tools for microRNA genomics." *Nucleic Acids Research* 36, no. (Database Issue) (2008): D154-D158.

Griffiths-Jones, S, R J Grocock, S van Dongen, A Bateman, and A J Enright. "miRBase: microRNA sequences, targets and gene nomenclature." *Nucleic Acids Research* 34, no. (Database Issue) (2006): D140-D144.

Grimson, Andrew, Kyle Kai-How Farth, Wendy K Johnston, Philip Garrett-Engele, Lee P Lim, and David P Bartel. "MicroRNA Targeting Specificity in Mammals: Determinants beyond Seed Pairing." *Molecular Cell* 27, no. 1 (July 2007): 91-105.

Grün, Dominic, Yi-Lu Wang, David Langenberger, Kristin C Gunsalus, and Nikolaus Rajewsky. "microRNA Target Predictions across Seven Drosophila Species and Comparison to Mammalian Targets." *PLoS Computational Biology* 1, no. 1 (June 2005): 51-56.

Hebb, Donald O. *The Organization of Behavior.* New York: Wiley & Sons, 1949.

Izquierdo, Ivan, Jorge H Medina, Monica R.M Vianna, Luciana A Izquierdo, and Daniela M Barros. "Separate mechanisms for short- and long-term memory." *Behavioral Brain Research*, 1999: 1-11.

Kandel, Eric R. "The Molecular Biology of Memory Storage: A Dialogue between Genes and Synapses." *Science* 294 (November 2001): 1030-1038.

Kaufmann, N, J DeProto, R Ranjan, H Wan, and D Van Vactor. "Drosophila liprin-alpha and the receptor phosphatase Dlar control synapse morphogenesis." *Neuron* 34, no. 1 (March 2002): 27-38.

Kelleher III, Raymond J, Arvind Govindarajan, and Susumu Tonegawa. "Translational Regulatory Mechanisms." *in Persistent Forms of Synaptic Plasticity* 44 (September 2004): 59-73.

Khvorova, A, A Reynolds, and S D Jayasena. "Functional siRNAs and miRNAs exhibit strand bias." *Cell*, 2003: 209-216.

Kim, J, A Krichevsky, Y Grad, G D Hayes, K S Kosik, and G M Church. "Identification of many microRNAs that copurify with polyribosomes in mammalian neurons." *Proceedings of the National Academy of Sciences of The United States of America* 101 (2004): 360-365.

Kim, V N, J Han, and M C Siomi. "Biogenesis of small RNAs in animals." *Nature Reviews in molecular biology*, 2009: 126-139.

Knucker, T, G R Siggins, and S Halpain. "Dynamic actin filaments are required for stable long-term potentiation (LTP) in area CA1 of the hippocampus." *Proceeding of the National Academy of Sciences of The United States of America*, 2000: 6856-6861.

Kogan, Jeffrey H, et al. "Spaced training induces normal long-term memory in CREB mutant mice." *Current Biology* 7 (1996): 1-11.

Koh, Y H, E Popova, U Thomas, L C Griffith, and V Budnik. "Regulation of DLG localization at synapses by CaMKII-dependent phosphorylation." *Cell*, no. 98 (1999): 353-363.

Kosik, K S, and A M Krichevsky. "The elegance of microRNAs: a neuronal perspective." *Neuron* 47 (2005): 779-782.

Kosik, Kenneth S. "The neuronal microRNA system." *Nature Review: Neuroscience* 7 (December 2006): 911-920.

Kozomara, A, and S Griffiths-Jones. "miRBase: integrating microRNA annotation and deep-sequencing data." *Nucleic Acids Research* 36, no. (Database Issue) (2011): D152-D157.

Krichevsky, A M, K S King, C P Donahue, K Khrapko, and K S Kosik. "A microRNA array reveals extensive regulationof microRNAs during brain development." *RNA* 9 (2003): 1274-1281.

Krug, M, B Lossner, and T Ott. "Anisomycin Blocks the Late Phase of Long-Term Potentiation in the Dentate Gyrus of Freely Moving Rats." *Brain Research Bulletin* 13 (1984): 39-42.

Lee, Y, et al. "MicroRNA genes are transcribed by RNA polymerase II." *EMBO journal*, 2004: 4051-4060.

Lewis, Benjamin P, Christopher B Burge, and David P Bartel. "Conserved Seed Pairing, Often Flanked by Adenosines, Indicates that Thousands of Human Genes are MicroRNA Targets." *Cell* 120 (2005): 15-20.

Livak, K J, and T D Schmittgen. "Analysis of relative gene expression data using real-time quantitative PCR and the 2(-Delta Delta C(T)) Method." *Methods* 4 (December 2001): 402-408.

Lund, E, S Guttinger, A Calado, J E Dahlberg, and U Kutay. "Nuclear export of microRNA precursors." *Science*, 2004: 95-98.

Luo, L. "Actin cytoskeletal regulator in neuronal morphogenesis and structural plasticity." *Annual Reviews in Cellular Developmental Biology*, 2002: 601-635.

Malinow, R, and R C Malenka. "AMPA receptor trafficking and synaptic plasticity." *Annual Reviews in Neuroscience*, 2002: 103-126.

Martin, S J, P D Gimwood, and R G.M. Morris. "Synaptic Plasticity and Memory: An Evaluation of the Hypothesis." *Annual Reviews in Neuroscience*, 2000: 649-711.

Mauelshagen, Juliane, Carolyn M Sherff, and Thomas J Carew. "Differential Induction of Long-Term Synaptic Facilitation by Spaced and Massed Applications of Serotonin at Sensory Neuron Synapses of *Aplysia californica*." *Learning & Memory* 5 (1998): 246-256.

Nagel, G, et al. "ChannelRhodopsin-1: a light-gated proton channel in green algae." *Science* 296 (2002): 2395-2398.

Nagel, Georg, et al. "Channelrhodopsin-2, a directly light-gated cation-selective membrane channel." *Proceedings of the National Academy of Sciences* 100, no. 24 (November 2003): 13940-13945.

Park, Chang Sin, and Shao-Jun Tang. "Regulation of microRNA Expressionby Induction of Bidirectional Synaptic Plasticity." *Journal of Molecular Neuroscience* 38 (2009): 50-56.

Pfaffl, M W. "A new mathematical model for relative quantification in real-time RT-PCR." *Nucleic Acids Research* 29, no. 9 (May 2001): e45.

Pfaffl, M W, A Tichopad, C Prgomet, and T P Neuvians. "Determination of stable housekeeping genes, differentially regulated target genes and sample integrity: BestKeeper--Excel-based tool using pair-wise correlations." *Biotechnology Letters*, no. 26 (2004): 509-515.

Rehmsmeier, M, P Steffen, M Hochsmann, and R Giegerich. "Fast and effective prediction of microRNA/target duplexes." *RNA* (The RNA Society) 10, no. 10 (October 2004): 1507-1517.

Roche, J P, M C Packard, S Moeckel-Cole, and V Budnik. "Regulation of synaptic plasticity and synaptic vesicle dynamics by the PDZ protein Scribble." *Journal of Neuroscience*, no. 22 (2002): 6471-6479.

Saito, Takaya, and Pal Saetrom. "MicroRNAs - targeting and target prediction (REVIEW)." *New Biotechnology*, 2010: 0000-0000.

Schacter, Daniel L. "Implicit Memory: History and Current Status." *Journal of Experimental Psychology: Learning, Memory, and Cognition*, 1987: 501-518.

Scharf, Matthew T, Newton H Woo, K Mathhew Lattal, Jennie Z Young, Peter V Nguyen, and Ted Abel. "Protein Synthesis Is Required for the Enhancement of Long-Term Potentiation and Long-Term Memory by Spaced Training." *Journal of Neurophysiology* 87 (2002): 2770-2777.

Schmies, G, M Engelhard, P G Wood, G Nagel, and E Bamberg. "Electrophysiological characterization of specific interactions between bacterial sensory rhodopsins and their transducers." *Proceedings of the National Academy of Sciences* 98, no. 4 (Feb 2001): 1555-1559.

Schratt, Gerhard M, et al. "A brain-specific microRNA regulates dendrite spine development." *Nature* 439 (January 2006): 283-289.

Schroll, Christian, et al. "Light-Induced Activation of Distinct Modulatory Neurons Triggers Appetitive or Aversive Learning in Drosophila Larvae." *Current Biology* 16, no. 7 (September 2006): 1741-1747.

Schuster, Christoph M. "Glutamatergic synapses of Drosophila neuromuscular junctions: a high-resolution model for the analysis of experience-dependent potentiation." *Cell Tissue Res* 326 (2006): 287-299.

Seggerson, Kathy, Lingjuan Tang, and Eric G Moss. "Two Genetic Circuits Repress the *Caenorhabditis elegans* Heterochromic Gene lin-28 after Translation Initation." *Developmental Biology* 243 (2002): 215-225.

Sempere, L F, S Freemantle, I Pitha-Rowe, E Moss, E Dmitrovsky, and V Ambros. "Expression profiling of mammalian microRNAs uncovers a subset of brain-expressed microRNAs with possible roles in murine and human neuronal differentiation." *Genome Biology* 5 (2004): R13.

Shuang, Zhao, and Liu Mo-Fang. "Mechanisms of microRNA-mediated gene regulation." *Science in China Series C: Life Sciences*, 2009: 1111-1116.

Silver, N, S Best, J Jiang, and S L Thein. "Selection of housekeeping genes for gene expression studies in human reticulocytes using real-time PCR." *BMC Molecular Biology* 7, no. 33 (2006).

Stark, Alexander, Julius Brennecke, Robert B Russell, and Stephen M Cohen. "Identification of Drosophila MicroRNA Targets." *PLoS Biology*, 2003: 397-409.

Steward, Oswald, and Erin M Schuman. "Protein Synthesis at Synaptic Sites on Dendrites." *Annual Review of Neuroscience* 24 (2001): 299-325.

Stewart, B A, H L Atwood, J J Renger, J Wang, and C F Wu. "Improved stability of Drosophila larval neuromuscular preparations in haemolymph-like physiological solutions." *Journal of Comparative Physiology A: Neuroethology, Sensory, Neural, and Behavioral Physiology* 175, no. 2 (1994): 179-191.

Tarnow, Eugen. "Short term memory may be the depletion of the readily releasable pool of presynaptic neurotransmitter vesicles of a metastable long term memory trace pattern." *Cognitive Neurodynamics*, 2009: 263-269.

Tulving, Endel. "Episodic memory: from mind to brain." *Annual Review in Psychology*, 2002: 1-25.

Tweedie, S, et al. "FlyBase: Enhancing Drosophila Gene Ontology annotations." *Nucleic Acids Research* 37 (2009): D555-D559.

Vandesompele, J, K De Preter, F Pattyn, B Poppe, and F Speleman. "Accurate normalization of real-time quantitative RT-PCR data by geometric averaging of multiple internal control genes." *Genome Biology*, 2002.

Vo, Ngan K, Xiaolu A Cambronne, and Richard H Goodman. "MicroRNA pathways in neural development and plasticity." *Current Opinion in Neurobiology* 20 (2010): 457-465.

Wahid, Fazli, Adeeb Shehzad, Taous Khan, and You Young Kim. "MicroRNAs: Synthesis, mechanism, function, and recent clinical trials." *Biochimica et Biophysica Acta*, 2010: 1231-1243.

Wang, Wang-Xia, et al. "Focus on RNA isolation: Obtaining RNA for microRNA (miRNA) expression profiling analyses of neural tissue." *Biochimica et Biophysica Acta* 1779 (2008): 749-757.

Wayman, Gary A, et al. "An activity-regulated microRNA controls dendritic plasticity by down-regulating p250GAP." *Proceedings of the National Academy of Sciences* 105, no. 26 (2008): 9093-9098.

Wibrand, Karin, et al. "Differential regulation of mature and precursor microRNA expression by NMDA and metabotropic glutamate receptor activation during LTP in the adult dendate gyrus in vivo." *European Journal of Neuroscience* 31 (2010): 636-645.

Wu, Gang-Yi, Karl Deisseroth, and Richard W Tsien. "Spaced stimuli stabilize MAPK pathway activation and its effects on dendritic morphology." *Nature Neuroscience* 4, no. 2 (February 2001): 151-158.

Xiao, Feifei, Zhixiang Zuo, Guoshuai Cai, Shuli Kang, Xiaolian Gao, and Tongbin Li. "miRecords: an integrated resource for microRNA-target interactions." *Nucleic Acids Research* 37, no. SI (January 2009): D105-D110.

Yu, Dinghui, David-Benjamin G Akalal, and Ronald L Davis. "Drosophila α/β Mushroom Body Neurons Form a Branch-Specific, Long-Term Cellular Memory Trace after Spaced Olfactory Conditioning." *Neuron*, no. 52 (2006): 845-855.

Zhang, Dr. *Evaluating Reference Genes Expression.* 2010. http://www.leonxie.com/referencegene.php?type=reference.

APPENDIX I

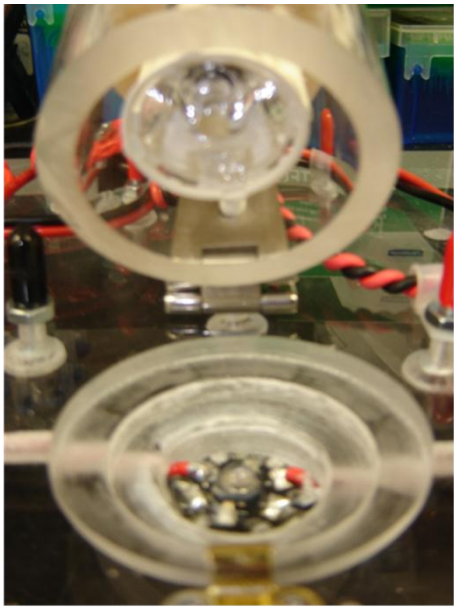

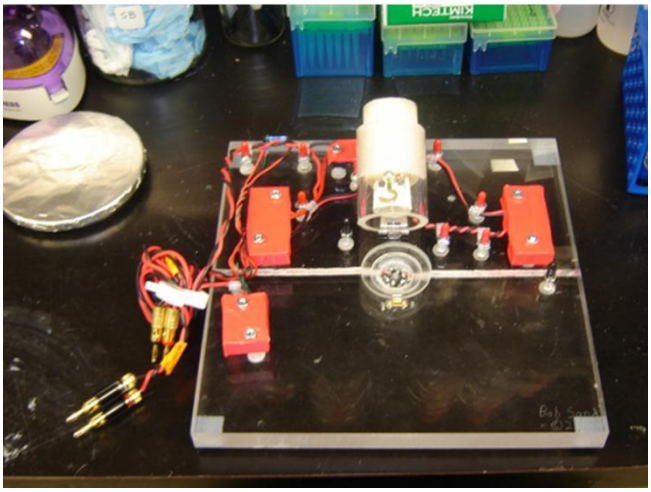

Supplemental Figure 1- The Channelrhodopsin stimulation apparatus. This custom built machine was used for all ChR2 related experiments. Shown here is the main stimulation apparatus with an additional picture showing the stimulation chamber.

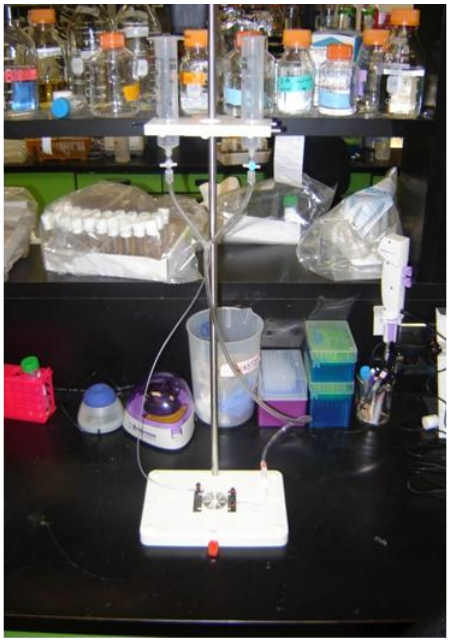

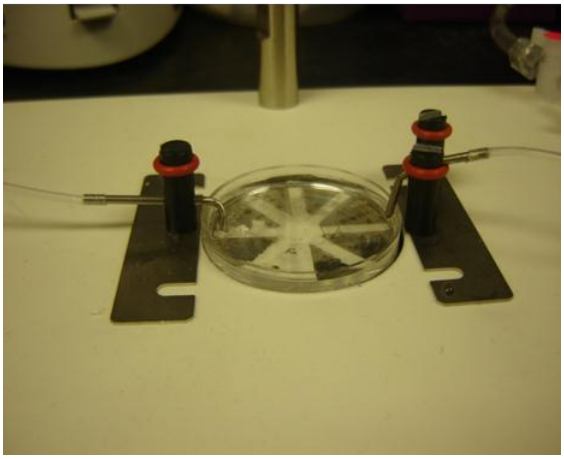

Supplemental Figure 2- High potassium stimulation perfusion apparatus. This apparatus was used for proper delivery of high and normal potassium HL-3 dissection buffers to dissection plates in order to perform spaced training.

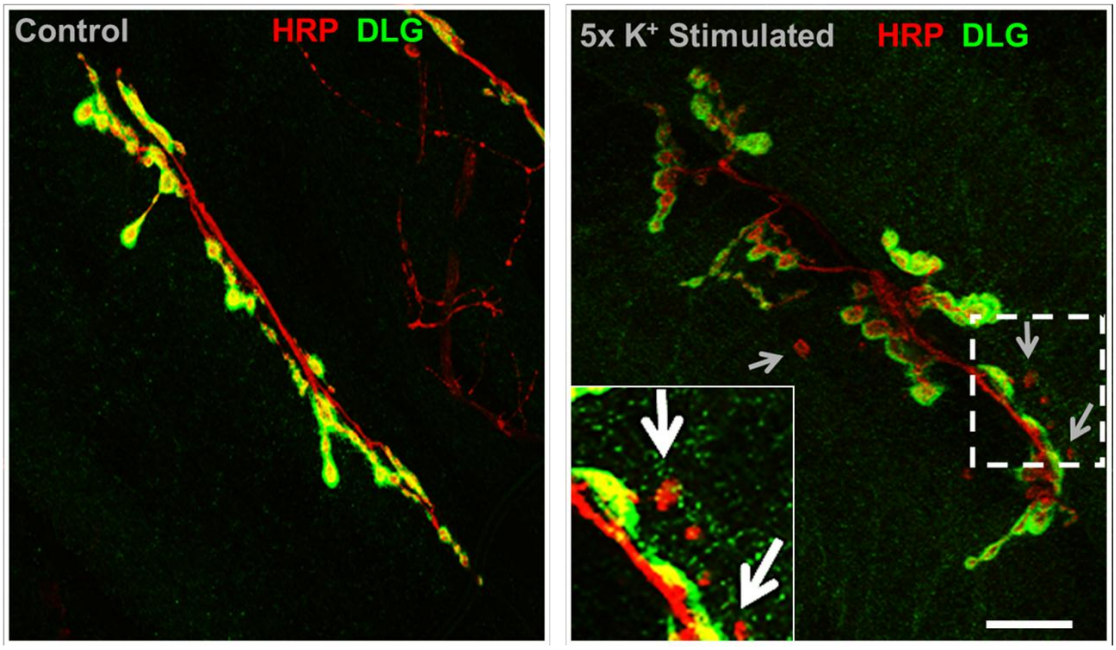

Supplemental Figure 3- High potassium spaced stimulation induces ghost bouton formation at the w^{1118} larval NMJ. Representative images of control and stimulated groups. Green= postsynaptic DLG, Red= presynaptic HRP.

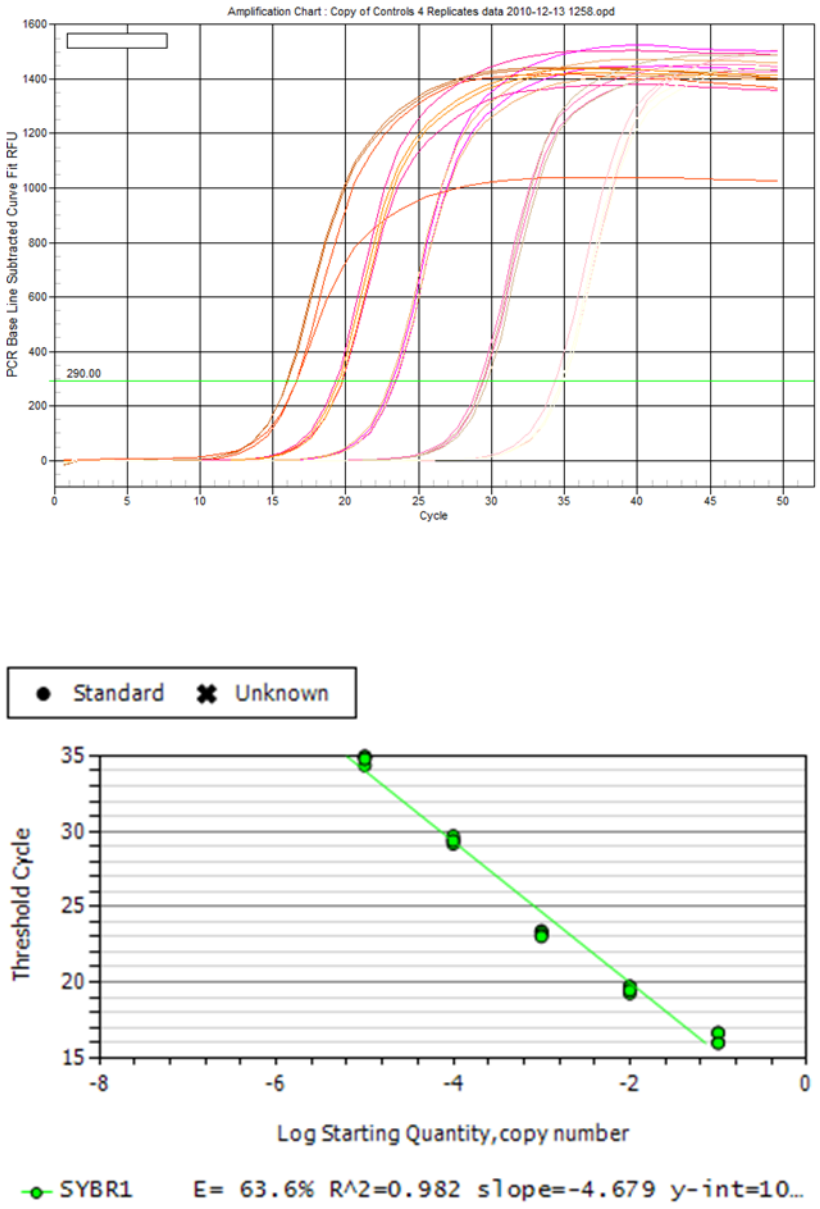

Supplemental Figure 4- Reference gene efficiency analysis. The representative graph depicts the raw amplification curve and standard curve for the U1 snRNA during the efficiency analysis. Efficiency and R^2 correlation values are shown in the standard curve image.

Good Primer Probe: U1 snRNA

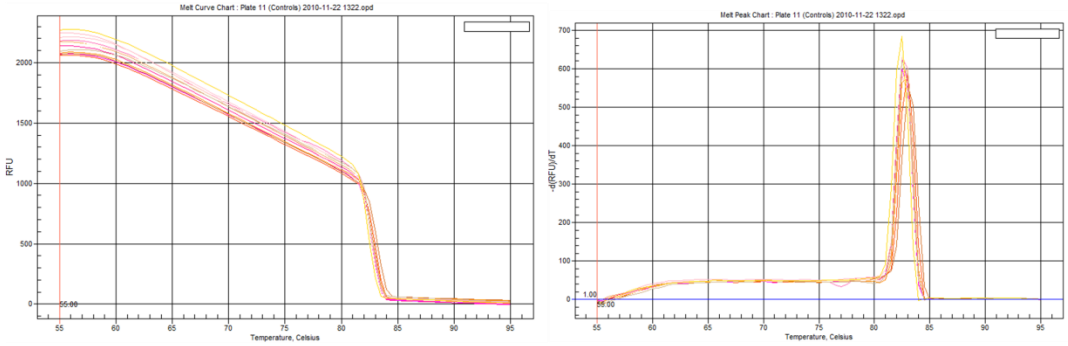

Bad Primer Probe: U12 snRNA

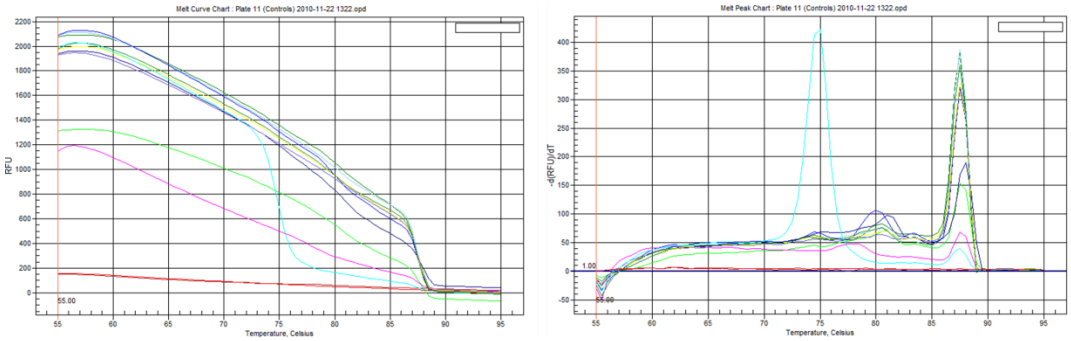

Supplemental Figure 5- Determination of melt curves for primer probes. In the optimization step of the experiment, melt curve information was retrieved from samples. A uniform curve and single peak indicates a single product formation (U1 snRNA) while a non-uniform curve and multi-peak analysis (U12 snRNA indicates a bad primer probe due to presence of multiple non-specific products.

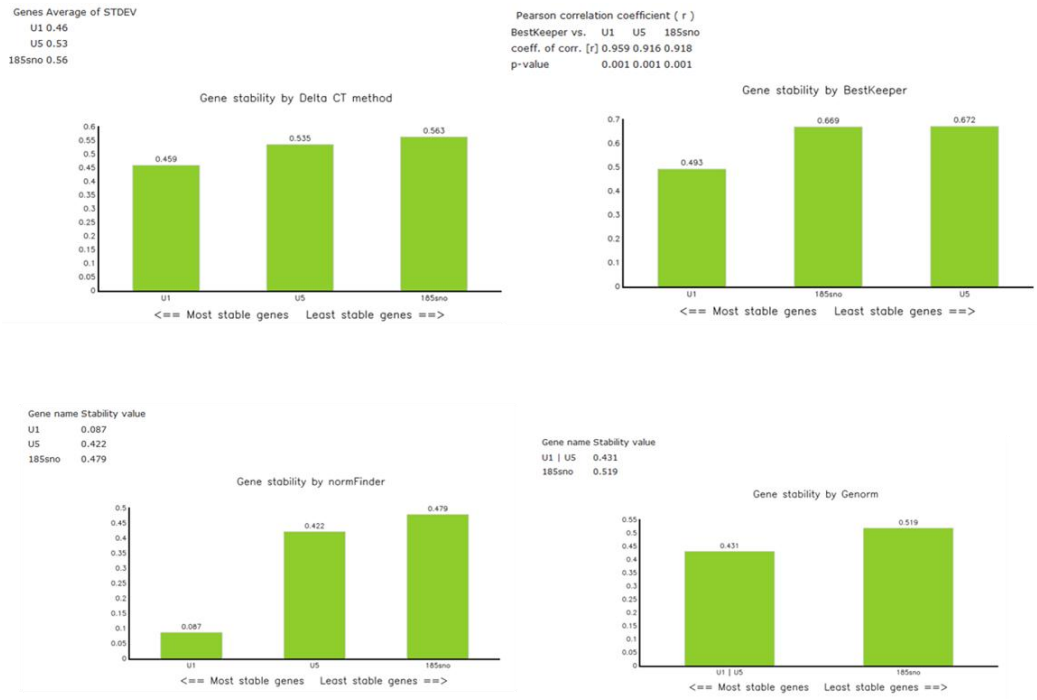

Supplemental Figure 6-Determination of reference gene stability. Using an all-inclusive web portal (Zhang 2010), which encompassed all depicted tests, Ct values from each of the 3 controls from all conditions and replicates were analyzed. These data came from the large-scale Canton S RT-qPCR study.

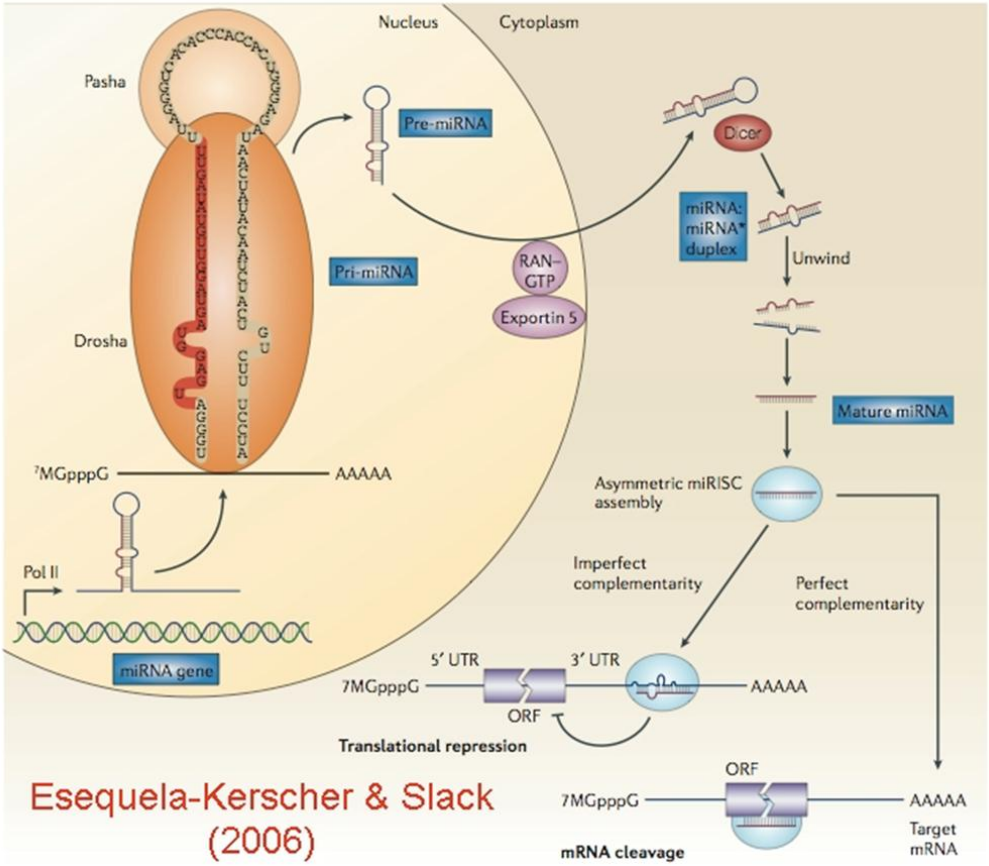

Supplemental Figure 7- The miRNA biogenesis pathway. In this cartoon taken from (Esequela-Kerscher, et al. 2006) the biogenesis and associated proteins relating to miRNA function are depicted.

APPENDIX II

A

miRNA Name	w^{1118} v. UAS-ChR2 (US) Fold Change (x)
miR-957	-1.82
miR-9a	1.74
miR-277	-1.63
miR-932	-1.60
miR-125	-1.56
miR-927	-1.56

B

miRNA Name	ChR2 US/S Fold Change (x)
miR-314	-1.44
miR-1	-1.22
miR-289	-1.20
miR-996	-1.19
miR-276*	1.19
miR-276b	1.19
miR-1013	-1.18
miR-276a	1.15
miR-14	-1.14
miR-970	-1.14
miR-263a	-1.14
Let-7	1.13
miR-iab-4-5p	-1.13
miR-9a	-1.12
miR-12	-1.12
miR-282	1.11
miR-92b	-1.11
miR-277	-1.10
miR-10*	-1.10
miR-1000	-1.10
miR-133	-1.10

Supplementary Table 1- microarray results summary. (A) This list contains all miRNAs with associated fold changes that underwent interactions between the w^{1118} genotype and the un-stimulated ChR2 genotype. (B) This is the summary table listing the initial 20 miRNA found to have >1.1-fold change in the ChR2 stimulated v. Un-stimulated microarray experiment.

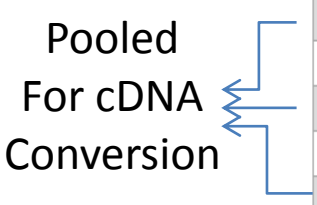

Well ID	Sample Name	RNA Area	RNA Concentration (ng/µl)	Ratio [28S:18S]	RQI	RQI Classification	RQI Alert
L	Ladder	317.19	160.00				
1	Sample 1	436.03	219.95	2.28	10.0	■	
2	Sample 2	38.78	19.56	2.28	9.7	■	
3	Sample 3	408.09	205.85	1.82	10.0	■	
4	Sample 4	40.33	20.34	1.05	9.2	■	
5	Sample 5	163.53	82.49	1.92	10.0	■	
6	Sample 6	3.12	1.57	1.34	N/A		Critical Anomaly

Supplemental Table 2- Determination of RNA integrity using the Bio-Rad Experion System. An example of results returned from the system. Particularly this run represents the samples used for efficiency and melt curve analysis. As denoted, these samples were pooled. Shown here is the summary table, displaying concentration and RQI values.

Well ID	Sample Name	RNA Area	RNA Concentration (ng/µl)	Ratio [28S/18S]	RQI	RQI Classification	RQI Alert
L	Ladder	289.58	160.00				
1	C1	259.21	143.22	1.22	9.6		
2	C1	234.54	129.59	0.96	8.8		
3	C2	349.34	193.02	0.77	8.3		
4	C2	347.06	191.76	0.00	10.0		
5	C3	514.49	284.27	1.49	9.8		
6	C3	480.69	265.59	1.16	9.6		
7	E1	552.15	305.08	1.02	9.4		
8	E1	569.03	314.41	0.50	7.6		
9	E2	419.26	231.65	0.94	8.8		
10	E2	414.91	229.25	0.75	8.3		
11	E3	561.44	310.21	0.35	10.0		
12	E3	477.67	263.93	1.57	9.8		

Supplemental Table 3- Experion analysis summary of RNA samples used for Canton S RT-qPCR Experiment. This table generated from the Experion software summarizes the concentration and RNA quality values (RQI) for the 6 input samples for the large-scale Canton S RT-qPCR study. All samples were run in duplicate, with C corresponding to RNA from a control sample, and E from a treated sample.

APPENDIX III

Drosophila melanogaster 3rd Instar Larval CNS Specific miRNAs			
Bantam	miR-79	miR-289	miR-997
Let-7	miR-92a	miR-304	miR-998
miR-1	miR-92b	miR-305	miR-999
miR-2a	miR-124	miR-306	miR-1000
miR-2b	miR-125	miR-307	miR-1001
miR-2c	miR-133	miR-308	miR-1003
miR-7	miR-184	miR-314	miR-1004
miR-8	miR-184*	miR-315	miR-1006
miR-9a	miR-190	miR-317	miR-1008
miR-9b	miR-219	miR-927	miR-1009
miR-9c	miR-252	miR-932	miR-1010
miR-10*	miR-263a	miR-957	miR-1012
miR-11	miR-263b	miR-958	miR-1013
miR-12	miR-275	miR-970	miR-1016
miR-13a	miR-276*	miR-974	miR-1017
miR-13b	miR-276a	miR-981	miR-iab-4-5p
miR-14	miR-276b	miR-987	Total: 79 miRNAs
miR-31a	miR-277	miR-988	
miR-31b	miR-279	miR-993	
miR-33	miR-282	miR-995	
miR-34	miR-284	miR-996	

Appendix III: The *Drosophila melanogaster* 3rd instar larval CNS miRNA expression profile. This table lists all CNS specific miRNAs present. This analysis reflects a 84% coverage of all miRNAs known in *Drosophila.*

APPENDIX IV

Drosophila melanogaster 3rd Instar Larval CNS Specific miRNAs			
Bantam	miR-79	miR-289	miR-997
Let-7	miR-92a	miR-304	miR-998
miR-1	miR-92b	miR-305	miR-999
miR-2a	miR-124	miR-306	miR-1000
miR-2b	miR-125	miR-307	miR-1001
miR-2c	miR-133	miR-308	miR-1003
miR-7	miR-184	miR-314	miR-1004
miR-8	miR-184*	miR-315	miR-1006
miR-9a	miR-190	miR-317	miR-1008
miR-9b	miR-219	miR-927	miR-1009
miR-9c	miR-252	miR-932	miR-1010
miR-10*	miR-263a	miR-957	miR-1012
miR-11	miR-263b	miR-958	miR-1013
miR-12	miR-275	miR-970	miR-1016
miR-13a	miR-276*	miR-974	miR-1017
miR-13b	miR-276a	miR-981	miR-iab-4-5p
miR-14	miR-276b	miR-987	Total: 79 miRNAs Good: 65 (82%) Bad: 14 (18%)
miR-31a	miR-277	miR-988	
miR-31b	miR-279	miR-993	
miR-33	miR-282	miR-995	
miR-34	miR-284	miR-996	

Appendix IV: Melt curve summary for all primer probes used. This summary list contains melt curve report summaries for every primer probe used in the miRNA experiments. A green label indicates the primer probe has a single-product (Good) whereas a red label indicates the primer prime has multi-product (Bad).